Master's thesis

NTNU
Norwegian University of Science and Technology
Faculty of Natural Sciences
Department of Materials Science and Engineering

Erlend Flø Gustad

Toward thin film organic coatings for corrosion protection of cultural heritage

Master's thesis in Materials Science and Engineering
Supervisor: Andreas Erbe
Co-supervisor: Vera de Bruyn-Ouboter
June 2022

NTNU
Norwegian University of
Science and Technology

Erlend Flø Gustad

Toward thin film organic coatings for corrosion protection of cultural heritage

Master's thesis in Materials Science and Engineering
Supervisor: Andreas Erbe
Co-supervisor: Vera de Bruyn-Ouboter
June 2022

Norwegian University of Science and Technology
Faculty of Natural Sciences
Department of Materials Science and Engineering

NTNU
Norwegian University of
Science and Technology

Abstract

Corrosion of metallic artifacts poses a significant challenge to the conservation of cultural heritage. At the Ringve / Rockheim Music Museum in Trondheim, Norway, corrosion damage has been observed on several musical instruments. Musical instruments pose particular challenges, as they contain certain material combinations in direct contact by design. The corrosion phenomena of iron on a square piano, a mandolin-banjo, and a surbahar are explored in this study. Corrosion protection systems based on organic thin films have been proposed as a solution with great potential. In this study, coating systems based on octadecyltrimethoxysilane (ODTMS), octadecylphosphonic acid (ODPA), and stearic acid (SA) on a steel substrate have been prepared from ethanol, isopropanol, and toluene solutions. Surface modification was verified by FT-IR spectroscopy and X-ray photoelectron spectroscopy (XPS).

Of the three thin film coating solutions, ODTMS deposited from an isopropanol solution showed the strongest inhibition of rust formation. The absence of substrate peaks in XPS analysis indicates that this system contains a layer that is thicker than a monolayer on the steel substrate. However, none of the coating systems were found to protect steel completely from the corrosive gas compounds from the degradation of cellulose nitrate. Organic compounds on the steel surface due to the contact with textiles, or volatile compounds from the wood casing are presented as possible explanations for the corrosion on the square piano. In the case of the mandolin-banjo and the surbahar, the presence of actively degrading cellulose nitrate was confirmed, providing an explanation for the observed corrosion phenomenon.

Sammendrag

Korrosjon av metall utgjør en betydelig utfordring for bevaring av museumsgjenstander, og ved Ringve / Rockheim musikkmuseum i Trondheim er det observert korrosjonsskader på flere musikkinstrumenter. Korrosjon av jern på et taffelpiano, en mandolinbanjo og en indisk surbahar utforskes i denne studien. Korrosjonsbeskyttelse basert på organiske tynnfilmer er ansett som en mulig løsning med stort potensial. I denne studien undersøkes tre forskjellige tynnfilms beleggsystemer basert på oktadecyltrimethoksysilan (ODTMS), oktadecylfosfonsyre (ODPA) og stearinsyre (SA) på substrater av stål påført fra organiske løsninger av etanol, isopropanol og toluen. Overflatemodifikasjon har blitt utforsket ved FT-IR-spektroskopi og røntgen-fotoelektron-spektroskopi. I tillegg har det blitt foretatt en undersøkelse av den korrosive effekten av cellulosenitrat på stål.

Av de tre tynnfilmbeleggsløsningene viste ODTMS avsatt fra en isopropanol-løsning det mest lovende resultatet, og dannet et lag på stålsubstratet med en tykkelse bestående av flere monolag. Ingen av belegningssystemene greide å beskytte stål tilstrekkelig mot korrosive gassforbindelser fra nedbrytning av cellulosenitrat. Observert korroson i taffelpiano foreslås å skyldes organiske forbindelser på ståloverflaten på grunn av kontakt med tekstiler, eller flyktige forbindelser fra treverk. For mandolinbanjo og surbahar ble tilstedeværelsen av aktivt nedbrytende cellulosenitrat bekreftet, og presentert som en forklaring på det observerte korrosjonsfenomenet.

Preface

This master thesis has been written as the Norwegian University of Science and Technology (NTNU) in Trondheim, at the department of Material Science and Engineering, during the spring of 2022. The resulting work is a collaboration between NTNU and Ringve / Rockheim music museum in Trondheim.

Acknowledgements

I would like to thank the following list of people for invaluable help and guidance throughout the project:

- My supervisor, prof. Andreas Erbe for sharing his knowledge and guiding me through the project.
- Co-supervisor, Vera de Bruyn-Ouboter, at Ringve music museum for sharing her knowledge and enthusiasm for the subject of this study.
- My classmates for good conversations and help when needed.
- Iman Yosuf for proofreading and active encouragement.
- Anita Storsve for practical help with lab equipment.
- Verner Håkonsen for helping me with XPS measurements and software.
- My family for their continuing support and encouragement.
- Lastly, i must thank my heavenly father who gave his only begotten son for the restitution of my sins.

Table of Contents

1 Introduction

1.1 Background and motivation

The general aim of conservation is to preserve historical objects over long periods [1]. Historical objects are often made up of different materials with different degradation processes. For example, musical instruments are cultural heritage objects containing metal and many types of organic material. Wherever there is metal, there is also corrosion. Therefore, corrosion in cultural heritage objects presents a significant challenge in the world of conservation.

This project is a collaboration with the Ringve / Rockheim Music Museum located in Trondheim, Norway. The museum has a collection of more than 2000 instruments with historical significance from all around the world, and the task of preserving these cultural heritage objects is a complex challenge. The historical instruments in Ringve / Rockheim are comprised of different materials and metals, in which corrosion has been observed. An understanding of these degradation processes and the various corrosion mechanisms occurring in the objects is necessary to mitigate the deterioration of cultural heritage items. Corrosion science is a field in constant development and with the aid of modern technology there is an ambition to explore possibilities of applying corrosion technology as a method to further advance conservation science.

1.2 Introduction to conservation

In general terms, conservation of artifacts follows two complementary approaches: preventive conservation through control of the environment, and remedial conservation through appropriate treatment to stabilize artifacts against degradation [1].

1.2.1 Conservation methodology

There are no clear lines that define the boundaries between proper and improper conservation treatments in general. An object must be evaluated individually and in its own context. However, a systematic methodology for conservation treatments of all kinds can be summed up in eight broad steps [2]:

1. Initial characterization of the object.
2. Reconstruct a history of the object.
3. Determine the ideal state of the object.
4. Decide on a realistic goal of treatment.
5. Choose the treatment methods and materials.
6. Prepare pre-treatment documentation.
7. Carry out the treatment.
8. Prepare final treatment documentation.

1.3 Scope of work

The general aim of this thesis is to understand the degradation mechanisms in the music instruments and to find possible methods to mitigate corrosion. In this work, two corrosion phenomena are investigated and a solution based on thin film technology for the protection of steel is explored. Some of the challenges when investigating museum objects is that they can not be dismantled, should preferably not be moved and sampling of material is very limited. This means that the possibility of testing the actual objects are limited to non-destructive tests and that creative solutions must be found to investigate the problems in different ways with minimal alteration of the instruments.

The first cultural heritage item under investigation in this work is the degradation of strings in a square piano manufactured in the period 1800 - 1825 [3]. On this piano, corrosion is observed in contact with textile fabric inside the piano housing. The inside of the piano is depicted in Figure 1.1 and 1.2. This thesis aims to build on the findings of the specialization project conducted in the fall of 2021 by Gustad [4]. Preliminary investigations in the specialization project worked towards the development of a model experiment with steel in contact with textile fabric. The aim of the experiment was to imitate the corrosion happening inside the square piano and obtain metal samples that could be characterized in more detail. The experiment is repeated in the present study, with samples coated with three kinds of thin films.

Figure 1.1: The square piano investigated in this project. Museum number: RMT 2012/02. Corrosion attack indicated by the white arrow. Photo: Ringve music museum. [3].

Figure 1.2: Close up image of corroded strings in contact with textile fabric.

The second phenomenon examined in this study is related to the decomposition of cellulose nitrate (CN), a precursor to modern day plastics. It is a light, strong, relatively stable and versatile material and its development was partly inspired by the need for cheaper materials for the production of billiard balls, traditionally produced from ivory [5]. Being a successful and cheap substitute, celluloid quickly found its way into the production of other applications containing ivory [6]. One such application was in musical instruments [7]. Being soluble in ether, solutions of cellulose nitrate also came to be used to produce coatings and lacquers [8]. As cellulose nitrate degrades, compounds are released which seem to have a corrosive effect on surrounding metal parts.

Two specific instruments in the Ringve collection suspected of being affected by this CN degration induced corrosion are a mandolin-banjo (museum id. RMT 721) from the 20^{th} century, and an indian instrument called a surbahar (Museum id. RMT 66/23) from around 1960[9], The banjo (Figure 1.3-1.4) has undergone significant corrosion in the strings at the nut of the instrument between the fret board and the headstock, as shown in Figure 1.4. This is proposed to be contact corrosion occurring due to the compound the nut is made of, and cellulose nitrate is suspected to be present.

Figure 1.3: The mandolin-banjo investigated in this work (museum number RMT 721)

Figure 1.4: Image of the mandolin-banjo instrument with increased magnification in which the corrosion occurring at the instrument nut is indicated by the red circle. Ringve /Rockheim music museum.

The surbahar (Figure 1.5, 1.6) has experienced corrosion in strings in a region above decorative

imitations of ivory as further indicated by Figure 1.6. The assumption is that cellulose nitrate degradation is responsible for the corrosion in the strings, due to the release of corrosive gases.

Figure 1.5: Image of a surbahar, an indian stringed instrument.

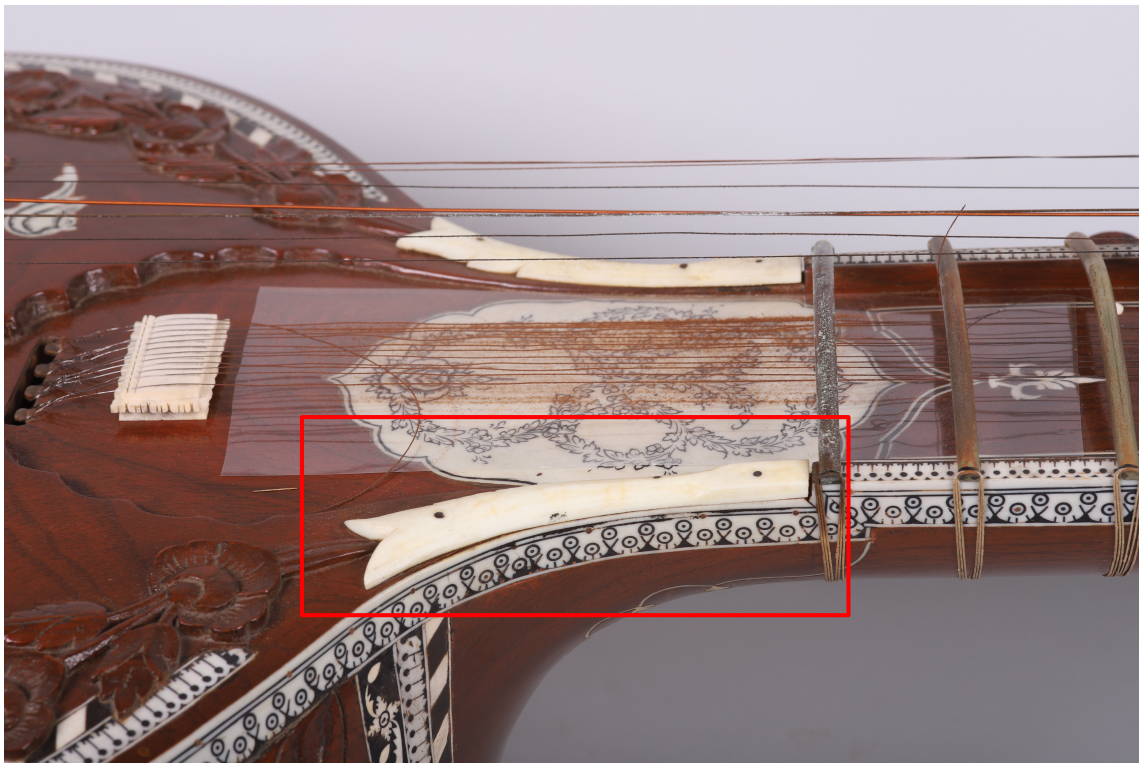

Figure 1.6: Region of corrosion occurring in surbahar instrument, indicated in the figure by the red rectangle.

2 Theory

2.1 Music wire

Historical music wire from the early 1800s was, of course, produced without the techniques and knowledge of alloying elements of today. One of the critical challenges of the production was making the wire as strong as possible to produce better tones and more sound [10]. Music wire was produced by the process of wire drawing, and the preferred raw material had to be high in both ductility and strength. The raw material in this period was remelted cast iron. The iron used to make music wire had a high phosphorous and low carbon content [10, 11]. This was a result of a process called the "Westphalian iron-refining process", which was unique to iron-refining for wire production. The composition of the music wire in the present study is currently unknown. However, given the preceding information, a reasonable assumption is that the wire is made of iron with relatively high phosphorous content and low carbon content.

Throughout the 19^{th} century, the quality of music wire improved significantly. Steel wire was introduced in the 1830s, and the introduction of alloying elements such as manganese allowed for the production of high-strength modern piano wire by the end of the century [10].

2.2 Corrosion

2.2.1 Basics

Corrosion is an important subject within the field of electrochemistry. It is described through redox reactions and includes the transfer of electrons and the change in oxidation states of the species involved. A general redox reaction is split into two half-reactions called oxidation and reduction reactions. In an oxidation reaction (also called anodic reaction), the oxidation state of some chemical element increases, as described in Equation 2.1 below:

$$\mathrm{M} \rightarrow \mathrm{M}^{+} + e^{-} \tag{2.1}$$

and conversely, in a reduction reaction (cathodic reaction) as shown in Equation 2.2, the oxidation state decreases [12]:

$$\mathrm{R} + e^{-} \rightarrow \mathrm{R}^{-} \tag{2.2}$$

The primary meaning of the word "corrosion" is the unwanted oxidation of metals by their environment. Fundamental thermodynamics governs this process and the aerobic oxidation,

$$\mathrm{M(s)} + \frac{b}{2a}\mathrm{O_2(air)} \rightarrow \frac{1}{a}\mathrm{M}_a\mathrm{O}_b\,\mathrm{(s)} \tag{2.3}$$

of nearly all metals is thermodynamically favorable [13]. In Equation 2.3, M denotes a metal, O denotes oxygen and a and b are stochiometric constants. The result of such a reaction is a thermodynamically stable metal oxide. In the case of steel, this will be iron oxides.

In a corrosion cell (a system where corrosion occurs), some elements must be present at all times. There must be an anode, a cathode, the possibility for transfer of electrons, and the possibility of transfer of ionic species. In most practical cases, water is the conductor of ionic species and is called the electrolyte [13].

2.2.2 Metal oxide

A metal oxide or hydroxide is the product of corrosion [14]. The surrounding environment and the chemistry of the metal oxide will significantly impact the propagation of the corrosion process. The purpose of this section is to emphasize the importance of pH in concerning corrosion. At different levels of pH and electrochemical potential, a metal can either be active (actively corroding), immune (not corroding), or passive (not corroding, or very slow corrosion) [15].

Under specific environmental conditions, some ordinarily active metals lose their chemical reactivity and become inert. This phenomenon is called passivity and is caused by the formation of a highly adherent and very thin oxide film on the metal surface. This serves as a protective barrier to further corrosion. For example, stainless steels are highly resistant to corrosion in a wide variety of conditions due to passivation. For most industrial steels, this is because they contain at least 11% chromium, a metal with a very stable metal oxide [16]. If, however, the metal oxide is porous, loose adherence, or is removed from the metal surface by the environment, it provides little protection, and the underlying metal remains chemically reactive.

The occurrence of passivation is often pH-dependent [13]. This is also the case for steel and iron. A potential-pH diagram, also known as a Pourbaix diagram, shows how metal and metal oxides behave at different potentials and pH. Figure 2.1 shows the Pourbaix diagram of iron. It shows that unprotected iron corrodes easily in neutral and acidic environments, while in basic environments, it passivates [15].

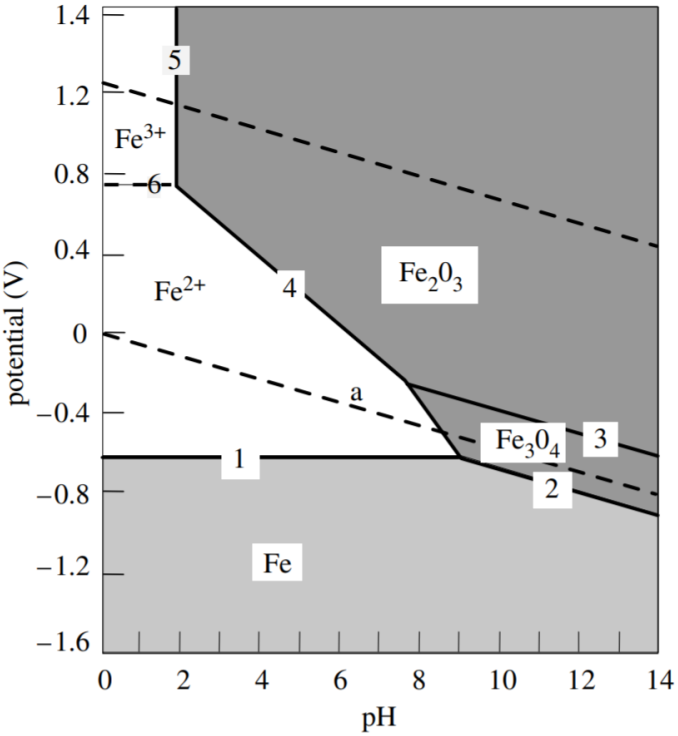

Figure 2.1: Simplified Pourbaix diagram of iron (T = 25 °C). The concentrations of the dissolved ionic species, Fe^{2+} and Fe^{3+} , are equal to 10^{-6}M [15].

2.2.3 The constituents of rust

The stoichiometry of rust approximately corresponds to the formula FeOOH, but in reality, rust is a mixture of different phases (crystalline and amorphous) of the oxides and hydroxides of iron. The chemical composition and structure of rust vary as a function of the climatic conditions and the length of exposure to the atmosphere. It also differs between the interior and exterior parts of the oxide layer. The three principal components of rust are [15]:

- α-FeOOH (geothite);
- γ-FeOOH (lepidococite);
- Fe_3O_4 (magnetite).

Rust layers typically comprise a relatively dense internal region on top of the metal, consisting of magnetite and amorphous phases of composition FeOOH, and a porous external region consisting mainly of lepidocrocite and goethite.

2.3 Atmospheric corrosion

The atmospheric corrosion process can be separated into different stages and processes that differ enormously in time scale. In the initial stages of the interaction between the solid and the atmosphere, an instant reaction of water vapor with the solid occurs, resulting in water adsorption

to the surface and the formation of a surface film. This process is closely related to the relative humidity and the hygroscopic properties of the substrate [1].

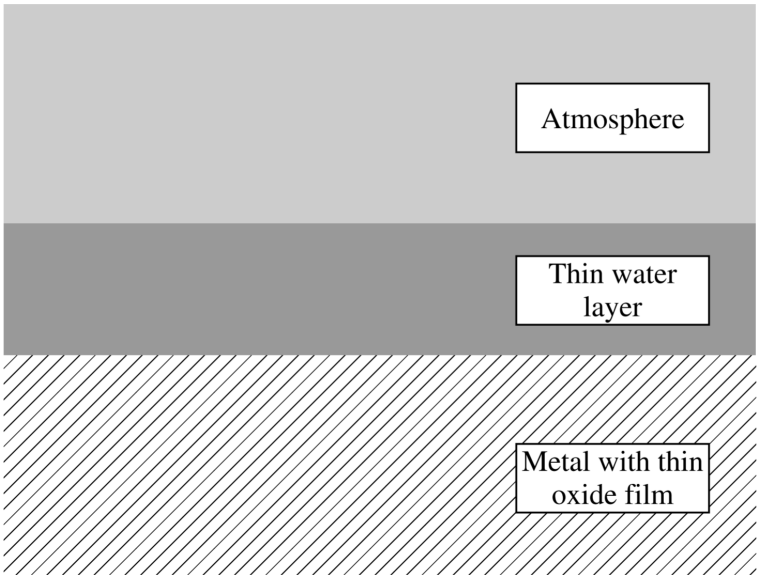

Figure 2.2: The interface that extends from the atmosphere over a thin water layer to the oxide covered metal [17].

In the intermediate stages of the process, the deposition of atmospheric constituents into the water film occurs, leading to several chemical reactions. Important reactions that may occur if the compounds are present are the transformation of sulfur dioxide SO_2 into sulfurous acid (H_2SO_3) or sulfuric acid (H_2SO_4), the transformation of NO_2 into nitric acid (HNO_3) and the dissociation of these acids. Subsequently, metal dissolution, ion-pairing, and nucleation of corrosion products occur. These processes happen in a time frame ranging from seconds to an hour [1].

The nucleated corrosion products grow with prolonged exposure until they cover the metal surface completely. As the layer of corrosion products, either a film or porous layer, grows, the transport of ions and electrons becomes more and more rate-determining concerning the overall corrosion process. When the corrosion products acquire characteristics that do not change much over time, the corroding material becomes characterized by a constant corrosion rate. The time needed to reach stationary atmospheric conditions may take several years or even decades, depending on the nature of the metal and its surroundings [1].

2.3.1 Atmospheric constituents

The composition of atmospheric air is approximately 77% N_2, 21% O_2, 1% Ar, 1-2% H_2O, 0.003% CO_2 (atomic percent) and traces of rare gases (He, Kr, etc.). In addition, it contains pollutants such as NO_x and SO_2, chloride ions, and airborne particles [15]. The indoor environment of a museum is determined by a large number of sources and sinks of air constituents, both gases and particles. There is always the transport from outdoors or other indoor rooms and direct indoor emission and production of pollutants through chemical reactions involving air constituents [1]. Constituents that are known to corrode metals under outdoor and indoor conditions include sulfur dioxide (SO_2), nitrogen dioxide (NO_2) ammonia (NH_3), hydrogen sulfide (H_2S) hydrogen peroxide (H_2O_2), ozone (O_3), aldehydes, organic acids, and aerosol particles, mainly sodium chloride (NaCl)

and ammonium sulfates ($(NH_4)_2SO_4$) or ($(NH_4)HSO_4$) [1]. Most gases exhibit lower concentrations inside than outside. However, in addition to some inorganic pollutants, concentrations of some organic compounds capable of causing corrosion are higher indoors than outdoor, such as formaldehyde (HCHO), acetaldehyde (CH_3CHO), formic acid (HCOOH), and acetic acid (CH_3COOH). They are either the result of emissions from various indoor materials such as wood, organic coatings, adhesives, and sealants or through indoor chemical reactions [1].

The release of organic acids into the air from the degradation of wooden objects has, in particular, been shown to affect cultural heritage objects [18]. In museum environments, pollution sources are often wood or wood products used in display case construction, but paint and acid curing silicone may also emit carboxylic acids. Situations where objects are displayed in relatively airtight cases thus allow a build-up of emitted compounds from the materials present in the case or the case itself [19]. in the present study, a similar situation may occurr, with a micro-climate inside the piano casing.

In every particular case, specific compounds may be present, but generally, the corrosivity of an atmosphere depends primarily on three parameters [1, 15]:

- relative humidity
- the SO_2 concentration
- the chloride concentration.

2.3.2 Relative humidity

The relative humidity is the most critical parameter for atmospheric corrosion because it determines if condensation can occur. For an atmosphere with a given absolute humidity, the relative humidity varies with temperature and surface topography. Condensed water on a metal surface forms an electrolyte with the salts deposited by pollutants and permits electrochemical reactions [15]. Reducing the relative humidity would therefore be beneficial for the corrosivity of the metal.

The picture becomes more complicated when dealing with cultural heritage objects because, more often than not, they contain non-metallic components. Therefore, the lower limit of relative humidity is set by breaking of fibers and embrittlement damage of moisture-containing materials, which occurs at relative humidity levels of less than 40 - 45%. Overall a relative humidity of 50 $\pm$ 5% seems to be a good compromise for diverse collections of material [1]. This has also been a strict international standard placed on museums containing cultural heritage collections. However, in recent years, this standard has been relaxed to a level of 40-60 % due to economic and ecological considerations [7]. In the storage facility containing the square piano under investigation in this work, the relative humidity is kept at 50 $\pm$ 5%[7].

2.4 Organic materials in contact with metals

The presence of organic material affects the corrosive environment of metals. Wood, leather, felts, and textiles are examples of materials that contain and produce compounds that present challenges for the conservation of cultural heritage objects [1]. Chemical treatment and the degradation processes of the respective materials must be considered to explain their corrosive properties. In

this project, felt and woven fabric used in pianos are investigated. These are in direct contact with the strings of the square piano.

Felt is a non-woven fibrous structure and can be produced from virtually any type of fiber. Wool is particularly well suited for felt making, and it is frequently blended as little as 10% with "non felting" natural or synthetic fibers. There are generally no adhesives used in the making of felts [20]. Woven cloths can be made of wool, but vegetable fibers such as cotton, hemp, flax, and ramie have also been used to a great extent in the textile industry.

Textile fibers are often hygroscopic, meaning they can absorb and retain water from a moist atmosphere [21]. In the context of corrosion, this usually has the effect of making the corrosive effects more aggressive.

Increased levels of organic compounds lead to corrosion products that often have metal-carboxylates as major constituents [1].

2.4.1 Wool

All-natural fibers derived from animals are built from proteins [20]. Wool is the fleece obtained from sheep and is mainly composed of the protein keratin [22]. The basic building block of a protein is an amino acid, which has the following basic formula [20, 23]:

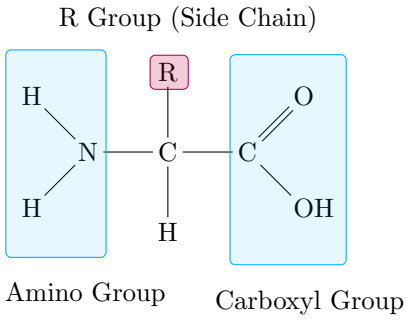

Keratin has a high content of the amino acid cystine [22]. Sulfur-containing amino acids such as this have been found to be efficient corrosion inhibitors [24, 25].

2.4.2 Vegetable fibers

The main constituent of vegetable fibers such as cotton and hemp is cellulose, a glucoside of glucose [20, 26], which can sometimes also serve as a corrosion inhibitor [27]. When cellulose degrades, however, the breakdown products are short-chain carboxylic acids, mainly formic acid (HCOOH), acetic acid (CH_3COOH), and propionic acid ($C_3H_6O_2$) which produce a corrosive environment [28].

2.4.3 Textile dyes

Dyes are mainly conjugated organic structures with an alternating system of single and double bonds within the molecule that impart the ability to absorb specific wavelengths of visible light. Hence the remaining light scattered by the dyed technical textile is perceived as colored. The coloration of technical textiles by dyeing is primarily intended for aesthetic purposes. However, it introduces other functional properties distinct from the aesthetic appeal of color [29, 30].

Different fibrous textiles have specific dyeing techniques associated with them, which might be interesting in the context of corrosion. Acid dyeing is common for wool fabrics, and these types of dyes contain acidic groups, usually sulphonate groups, either as -SO_3Na or -SO_3H groups. Carboxyl groups (-COOH) can sometimes also be incorporated [29].

Mordant dyes are another type used for wool fabrics, where the final result is a Cr^{3+} complex inside the fiber. Sulfide dyes are also an alternative for the dyeing of fabrics. In addition, there is a range of chemical compounds used as pigments [29].

2.5 Cellulose nitrate

A substance of interest with regards to corrosion of cultural heritage is cellulose nitrate, a precursor to today's polymeric plastic materials [8]. It is produced by nitration of either cotton lint or wood pulp cellulose, where the hydroxyl groups on the cellulose backbone are replaced with nitrate esters. Figure 2.3 shows the repeating unit of cellulose nitrate. One drawback of the compound is that it is combustible and is thus regarded as a fire hazard [31]. Adding sulfuric acid (H_2SO_4) to the nitrating mixture provides stabilization against detonations. The H_2SO_4 also acts as a catalyst in the nitration reaction, creating pathways for the nitrate groups provided by nitric acid (HNO_3) [32].

A common procedure for identifying cellulose nitrate in cultural heritage objects is the diphenylamine spot test [33, 34]. However, infrared spectroscopy is by far the most accurate means to identify cellulose nitrate[6].

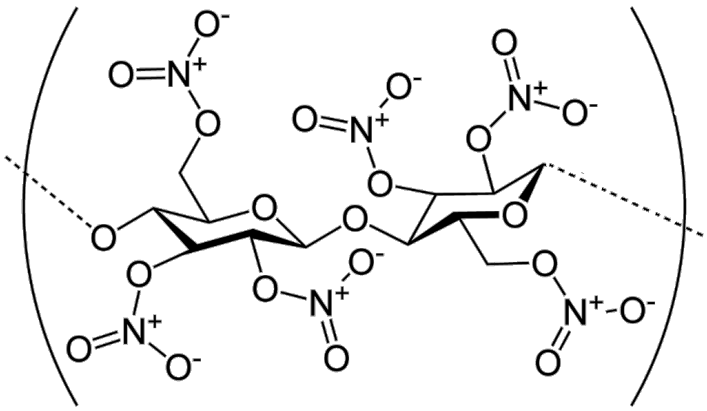

Figure 2.3: Repeating unit of cellulose nitrate compound.

The aging behavior of cellulose nitrate shows itself visually by cracking and yellowing [31]. Under low power magnification, one may see distinctive weathering patterns of celluloid nitrate, consisting of a series of conchoidal fractures forming a checked pattern [6]. Further signs of degradation are the rapid deterioration of mechanical properties.

For cellulose nitrate, experimental evidence has shown that mechanisms based on radical propagation are dominant in the degradation process [5]. This means that once a reactive free radical is generated, it can react with stable molecules to form new free radicals. These new free radicals go on to generate yet more free radicals, and so on [26]. It has been proved that cellulose nitrate degradation occurs step-wise through side and main chain scission, which leads to a separation of a mixture of nitrogen oxides, carbon monoxide, and carbon dioxide. The nitrogen oxides form nitric acid if moisture is present [31, 35, 36].

2.6 The requirements of a coating for the preservation of cultural heritage

Extensive efforts have been invested in developing strategies that can either isolate the metal from its environment or decrease the corrosion rate to an acceptable level. Many corrosion-resistant coating solutions have been employed during the last several decades, such as oils and greases, conversion coatings, varnishes, and metallic and organic coatings. However, none satisfactorily fulfill the requirements in the field of cultural heritage, which can be summarized by the following criteria [37]:

- Respect for the visual appearance.
- Ease of application.
- Reversibility, i.e., ease of removal.
- Environmentally friendly chemicals.

One common compound used for coating cultural heritage objects is "Paraloid B72", a copolymer of methyl acrylate and ethyl methacrylate [38]. Conservators apply them as coatings, consolidants, or adhesives. It is used because of its reversibility, long-term stability, easy applicability (it has negligible harmful volatile emission), and good adhesion to the substrate. However, it is an inherently hydrophilic material and has a relatively high gas permeability. Nonetheless, Paraloid B72 is often used as a reference when introducing new materials in the conservation practice [39].

2.7 Thin film technology

Thin film technology is the exploration of coatings with thicknesses on the sub-micrometre scale [40]. These coatings may protect the surface in different ways depending on the interaction with the substrate and the chemistry of the coating itself. In the case of anti-corrosion coatings, the mechanisms by which they operate can be divided into three categories: barrier creation between substrate metallic material and the surrounding environments, the inhibition of the corrosion process, and the coating acting as a sacrificial material [41].

2.7.1 Self-assembled monolayers

Self-assembled monolayers (SAMs) are highly ordered, and close-packed molecules formed by adsorption of organic molecules onto a solid substrate through a self-assembly process [37, 42]. The general molecules used to produce an organic SAM has three main characteristics [43, 44]:

1. a functional group that chemically bonds to the surface, responsible for the layer adhesion to the substrate (head group), and is specific for different substrates.
2. an aliphatic chain, which acts in the self-organization process.
3. a functional group exposed on top of the layer (endgroup).

A schematic represation of a self-assembled monolayer is provided in Figure 2.4 below.

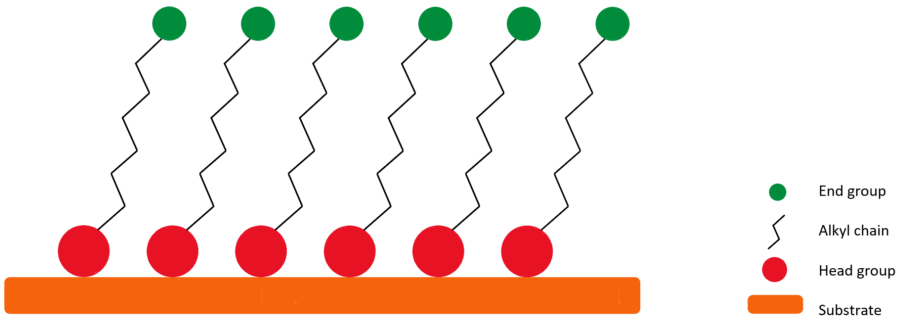

Figure 2.4: Schematic representation of a SAM consisting of a headgroup, an alkyl chain and an end group.

The choice of headgroup is critical for the stability of SAMs [45]. The "pair" of the chemisorbing headgroup and the substrate is regarded as the defining feature, while the rest of the molecule can be almost freely chosen [44]. Thus, it is common to classify SAMs according to their headgroup, such as silanes, thiols, phosphonates, and more.

The endgroup, which interacts with the environment, can be chosen based on the desired requirements of the coated surface. This could, for example, result in a hydrophilic or hydrophobic surface or make it electroactive [37]. It is also possible to leave out the endgroup from the SAM, leaving only a methyl group at the end of the molecule. This results in a simpler SAM where the alkyl chain length heavily influences its properties.

The influence of alkyl chain length on the corrosion protection of the SAM is significant [46]. To act as a barrier between the metal and the environment, it is important that the alkyl chains have a dense and ordered structure, which is harder to obtain with short chains [46]. The "hydrophobic barrier" effect is reported to require an alkyl chain length at least in the range of C_{12-18} [47–49]. In the case of very long chain lengths, gauche defects and entropic contributions will become increasingly problematic [44].

In the present study, three simple types of SAMs with different head groups are explored, one organosilane, one phosphonate, and one carboxylic acid. The different SAMs were selected based on promising findings from the literature. For the sake of simplicity, the aliphatic chain was of equal length for the three different SAMs, and none of them had a functional group at the end.

2.7.2 Organosilanes

Organosilanes are compounds with the general formula $R-(CH_2)_n-Si-X_3$, where R is a functional group and X is a readily hydrolyzable group, such as chloro-, alkoxy- (methoxy-, ethoxy-, or acetoxy ($OCOCH_3$) [50]. The defining element of these compounds is the silicon atom in the headgroup. Silicon has a normal oxidation state like that of carbon but is slightly more electropositive, resulting in bond strengths, bond angles, and bond lengths that differ from most organic compounds. As a result, such "inorganic" compounds often display enhanced properties, including thermal endurance, chemical or moisture resistance, increased mechanical strength, and electrical performance over materials with a completely organic nature [51].

Organosilanes are commercially available and can form self-organizing siloxane surface nanolayers upon adsorption on metals [51]. They are used as adhesion promoters or cross-linking agents in the paint industry, and the addition of small amounts of silane significantly improves the polymer adhesion to the surfaces of fiberglass, metals, and other inorganic substrates [50].

The interaction of silanes with the metal surface depends on the metal surface's condition. A surface with a high density of hydroxyl ($-OH$) groups will be preffered [51].

Silanes will eventually be broken down by water reaching the metal-silane interface, where it reverses the Si-O-Me bond formed by hydrolysis to protect the metal[42].

The organosilane chosen in the present study is octadecyltrimethoxysilane (ODTMS), which has a chemical composition of $C_{21}H_{46}O_3Si$. The terminals of ODTMS that end with methoxy groups are reported to possess high water repellent properties [52]. With the methyl terminal group of the alkyl chain oriented outwards in an ordered monolayer, the access of water to the methylene bond is inhibited [53]. A successful formation of a high-quality densely packed film on mild steel using ODTMS has been shown to provide durable protection against microbial corrosion [54]. The supposed interaction at the metal oxide-silane interface is shown in Figure 2.5. The figure depicts a surface siloxane layer bound to the metal oxide surface by covalent Si-O-Me bonds [44, 50, 55, 56].

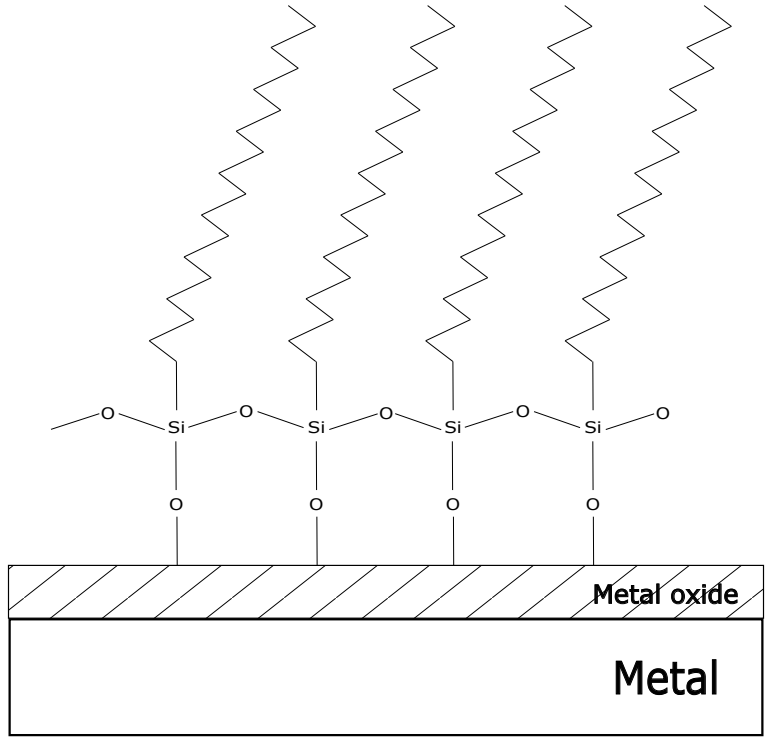

Figure 2.5: Schematic representation of the metal oxide-silane interface. The molecules are bound to the surface by covalent Si-O-Me bonds and connected by Si-O-Si bridges.

2.8 Phosphonates

Phosphonates form an extensive class of phosphorus-containing organic compounds having the general formula $R-P(O)(OH)_2$. Some of these can form self-assembled monolayers, which are interesting for the passivation of metal components. In recent years, the range of phosphonic compounds used for modification of technical metals and methods of its implementation has increased significantly [46]. For organophosphorus compounds to be suitable for surface modification, the anchoring phosphorus atom should be bound to reactive groups such as OH, OR, or halogens. The most appropriate organophosphorus modifiers of oxide surfaces are phosphorus(V) acids (phosphonic and phosphinic acids) and their derivatives [57].

In the present study, octadecylphosphonic acid (ODPA) is investigated as a possible coating for historical musical instruments. This compound has the chemical formula $C_{18}H_{39}O_3P$. The terminals of the phosphorous-containing headgroup consist of two singly-bound hydroxyl groups and one oxygen via a double bond. Thus, the bonding to the surface can be either mono, bi, or tri-dentate, as illustrated in Figure 2.6 [45]. Similar to ODTMS, this monophosphonic compound has a long alkyl chain which makes the SAM more hydrophobic than phosphonic acids with shorter chains [45, 58].

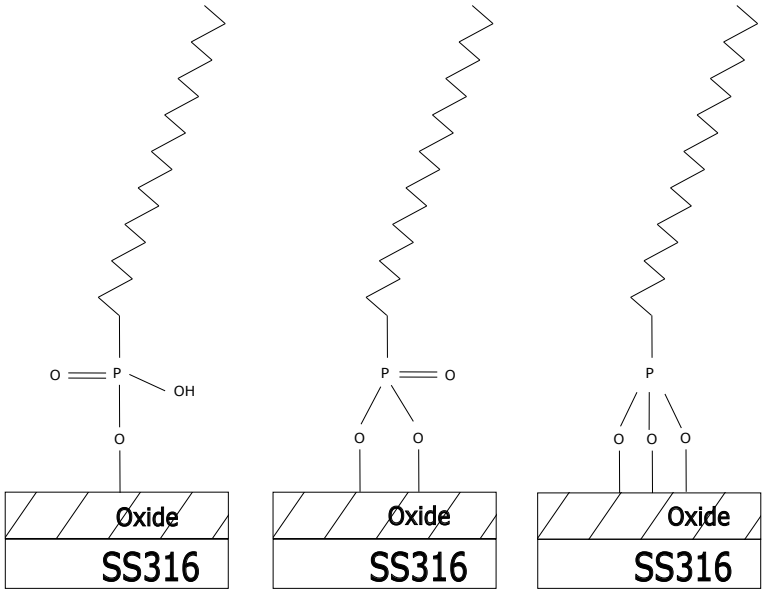

Figure 2.6: Monodentate, bidentate, and tridentate bonding modes of ODPA on stainless steel 316L.

2.8.1 SAMs from Carboxylic acids

SAMs from Carboxylic acids are compounds with the general formula in the present study, a similar situation may occurr, with a micro-climate inside the piano casing.$R-(CH_2)_n-COOH$ and are attracting attention for coating various metal and metal oxide surfaces[37, 59]. Earlier it was pointed out that the presence of carboxylic acids acted as a corrosion promoter. Thus it may seem counter-intuitive to assume that carboxylic acids can be used as a corrosion inhibitor. In the presence of a thin water layer, short-chain carboxylic acids distributed on the surface lower the pH, making the environment harmful [1]. The deliberate construction of a stable monolayer of long-chain carboxylic acids would create a barrier, preventing harmful species from reaching the metal oxide layer [60].

Stearic acid (SA), also known as octadecanoic acid or octadecyl carboxylic acid, has been chosen for the present study. It has the chemical formula $CH_3(CH_2)_{16}COOH$. The mechanism for the headgroup (COOH) interaction with the oxide layer has been described as an acid-base reaction, forming a surface salt between the carboxylate anion and a surface metal cation. Furthermore, the bonding mode for long-chain alkanoic acid has been shown to be predominately bidentate, as illustrated in Figure [61, 62].

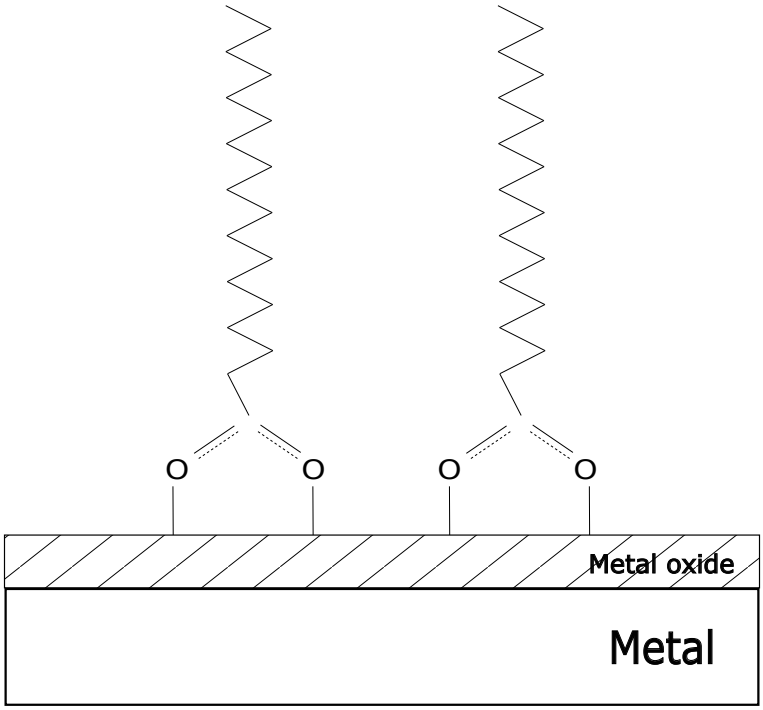

Figure 2.7: Schematic of a bidentate bonding mode of SA on metal surface.

Preparation of thin films on steel There are several ways of obtaining thin films on metal substrates. For example, spin-coating is a popular preparation method for thin polymer films. The most common methods available include the following [43, 44]:

- Langmuir-Blodgett films. These are prepared by transferring Langmuir amphiphilic molecules spread on a liquid surface onto a solid substrate while the hydrophobic endgroup sticks out on the other side.
- Growth from solution. Here, chemisorption of the headgroups with a specific affinity to the substrate leads to the formation of ordered thin films on a substrate submerged into a solution.
- Vapor deposition. Here the film is formed from the gas phase in vacuum.

Growth from solution is the traditional preparation method for SAMs and was used in this project. Its advantage is the ease of use, it's an environmentally friendly option, the potential to coat objects with complex shapes, and the plethora of literature on the subject.

2.9 Methodology and methods

Most techniques for analysis of corroded surfaces are based on the bombardment of the sample with particles such as photons, electrons, or ions [1]. The following section presents a brief introduction to the techniques used in this study for those without prior knowledge.

X-ray photoelectron spectroscopy (XPS): Here, the material surface is irradiated by a monochromatic beam of x-rays. The X-rays interact with the material surface. Because each element in

the sample emits a characteristic spectrum of electrons, the overall recorded spectrum provides an elemental analysis of the investigated surface [1].

Infrared spectroscopy (IR): This method gives information on molecular structure through the frequencies of the normal modes of vibration of the molecule. A normal mode is one where each atom executes a simple harmonic oscillation about its equilibrium position. The method measures the amount of IR radiation that passes through the sample versus the radiation wavelength [63].

Raman spectroscopy: This is a different way of measuring molecular vibrations, but here the sample is illuminated with a laser beam, and the range of vibrational modes detected is different from IR [64].

3 Experimental

The following chapter describes the materials, methods, and characterisation techniques used for experiments and analyses in this study. The present work is partially a continuation of the project work conducted by the author from the fall of 2021 [4].

3.1 Materials

3.1.1 Steel

The steel used in the experiment is low-carbon cold-rolled steel manufactured for the purpose of corrosion testing in the automotive industry. The product name is "Gardobond 26s/6800 MBS 21" and is distributed by Chemetal GmbH, a company delivering solutions for applied surface technology. The surface finish has an average roughness value, [R_a] , of 1.1 - 1.6 µm. The elemental composition of the steel is given in Table 3.1 below. The steel was cut into pieces of 2x2 cm, as shown in Figure 3.1, and had a thickness of (0.80 ± 0.03) mm with average roughness value $R_{Pc} = 1.1 - 1.6$µm.

Table 3.1: Elemental composition of steel samples used in this study.

	Element (at%)							
	C	**Si**	**Mn**	**P**	**S**	**Al**	**Ti**	**Cu**
Gardobond MBS	0.06	0.50	0.40	0.025	0.020	0.010	0.30	0.20

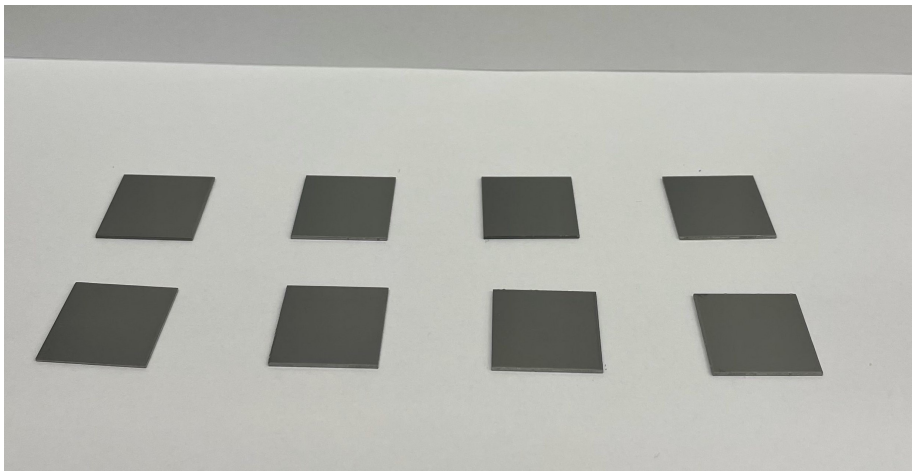

Figure 3.1: Steel samples (Gardobond 26s/6800 MBS 21) cut into 2x2 cm pieces. The thickness and average roughness value (R_{Pc}) of the steel was 0.80 ± 0.03 mm and $R_{Pc} = 1.1 - 1.6$µm, respectively.

3.1.2 Textiles

Two types of textiles are used in this project. One red wool felt and white fabric, which is mainly cotton. The textiles were retrieved from the conservation workshop at Ringve / Rockheim Music

Museum. The origin and exact composition, as well as processing and dyeing of the textiles used in the experiment, are unknown. However, the materials were bought from a dealer of piano parts in the 1990s [7]. These textiles are considered suitable substitutes for the textile material in pianos and seem reasonable to use in the present study.

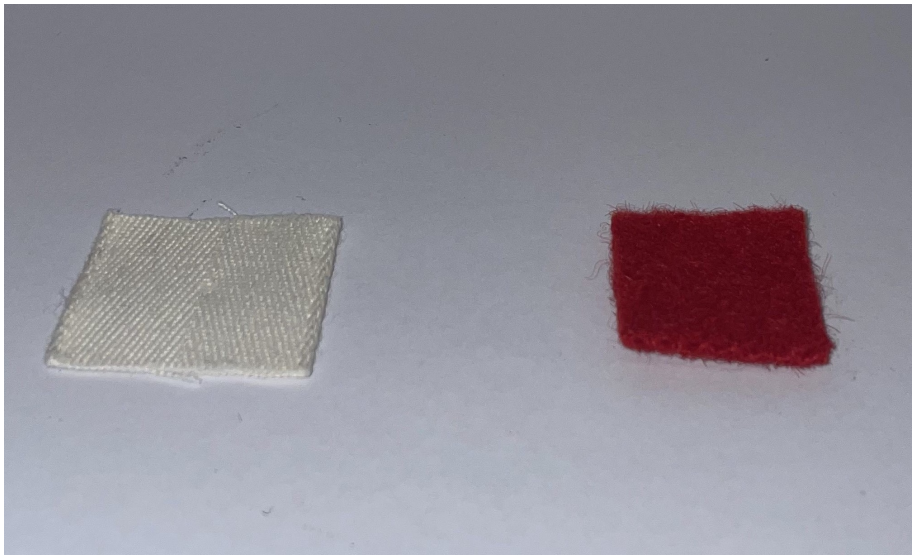

Figure 3.2: Image taken of the textile fabric cut into pieces of approximately 2x2 cm.

3.1.3 Cellulose nitrate

Two plates of cellulose nitrate were subjects of investigation in this study. Firstly, a scratchplate (museum number Rock 2725) taken from an electric guitar at the Rockheim Music Museum showed clear signs of degradation. The plate is depicted in Figure 3.7. The second plate used is sampled from the grill of an accordion, and an image of the plate is provided in Figure 3.8. However, this piece is not part of the museum's collection but was chosen for experiments because the material was confirmed to be cellulose nitrate before the experiments started and were visually not yet in a state of deterioration.

In addition, the two stringed instruments introduced in Section 1.3, the mandolin-banjo and surbahar (Figures 1.3 and 1.5 respectively), were investigated for confirmation of the construction material. They were subjected to a diphenylamine spot test, and analyzed in FTIR spectroscopy by attenuated total reflectance (ATR).

3.2 Investigation of square piano

One experiment was conducted in order to test steel in contact with textile fabric in different conditions, piano atmosphere and lab atmosphere. The experimental design was made to imitate the contact between wire and textile, as shown in Figure 1.2. This experiment was conducted in the preceding project work from the fall of 2021, where samples were tested without coating. For a discussion about the validity of the model, see the project report [4]. The present study tested samples coated with three different kinds of self-assembled monolayers in similar conditions.

The textile fabric was cut into pieces of about 2.5x2.5 cm as shown in Figure 3.2. No further

preparation was done. The sample size was chosen for practical purposes, both in the execution of the experiment and the subsequent analysis of the samples.

Four flat steel samples were placed inside the square piano in the storage facility of the museum, one coated with ODTMS, one with ODPA, and one with SA. All three coating procedures used isopropanol as solvent. One sample was not coated. All four were in contact with white cotton fabric. To ensure that there was sufficient contact between textile and steel, a provisional weight was added, comprised of 100 g of lead in a glass container. The samples were mounted as shown in Figure 3.3. Relative humidity of the environment in the storage facility is kept relatively constant at RH 50% and was. To imitate this condition in the lab, four samples were placed in a glass desiccator in a similar fashion, as shown in Figure 3.4. The relative humidity was controlled inside the desiccator using a $Ca(NO_3)_2 \cdot 4\,H_2O$ salt solution. A saturated salt solution was prepared by putting 145 g salt into a petri dish, followed by addition of distilled water, as depicted in Figure 3.5. The humidity inside the desiccator was confirmed at RH 50% at equilibrium.

Figure 3.3: Steel and fabric weighted down by lead weights inside square piano in the storage facility of the museum. The samples were each prepared with different coatings: ODTMS, ODP, SA and a final uncoated sample.

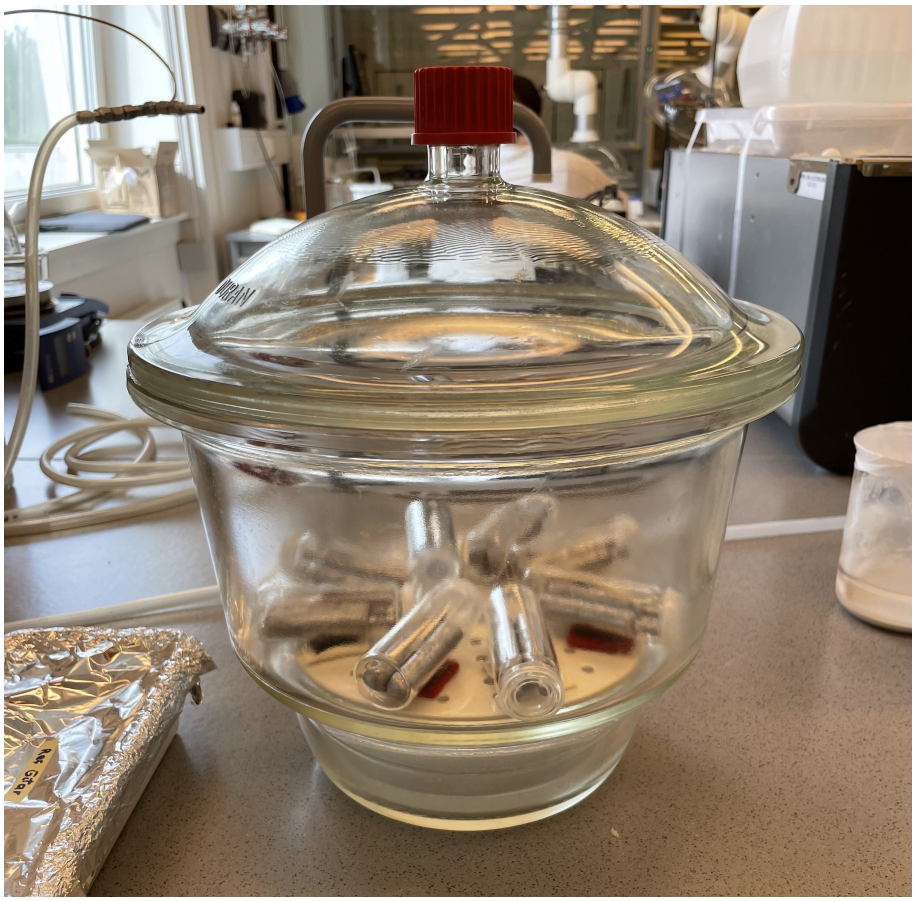

Figure 3.4: Steel and fabric inside an desiccator maintaining a constant relative humidity of 50%. The lead weights ($m = 100\ g$), which were used to ensure contact between the fabric and steel, are also visible in the image.

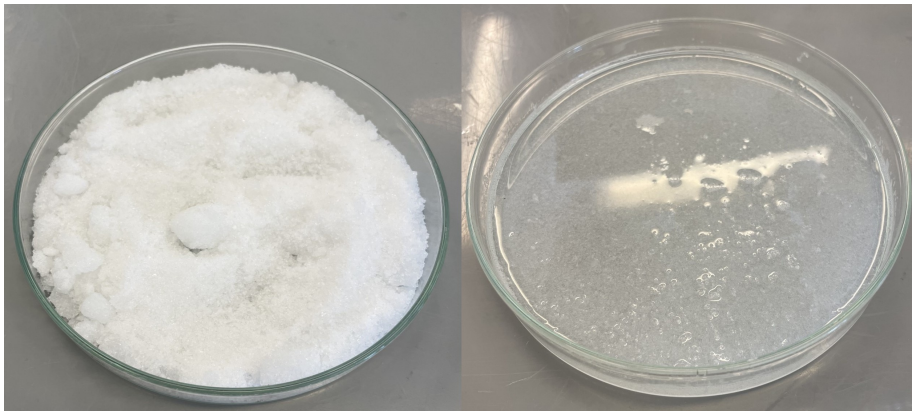

Figure 3.5: A saturated salt solution comprising of calcium nitrate tetrahydrate ($Ca(NO_3)_2 \cdot 4\,H_2O$) and water was prepared to enable control of humidity inside the desiccator. The image on the left shows the petri dish prior to the addition of water, and on the right the obtained saturated salt solution is shown.

The treatment of the steel samples can be summarized in the flowchart in Figure 3.6. Before the start of the experiment, the samples were ultrasonically cleaned in ethanol for 15 minutes. Subsequently, they were chemically cleaned for 2 minutes in a 2.5 molar sodium hydroxide (NaOH) solution at room temperature. They were then examined in Fourier-transform Infrared (FTIR)

spectroscopy grazing incidence (GI) to verify that they had the same surface conditions. At the end of the experiment, the samples were taken out and first examined with FTIR and finally examined using X-ray Photoelectron Spectroscopy (XPS).

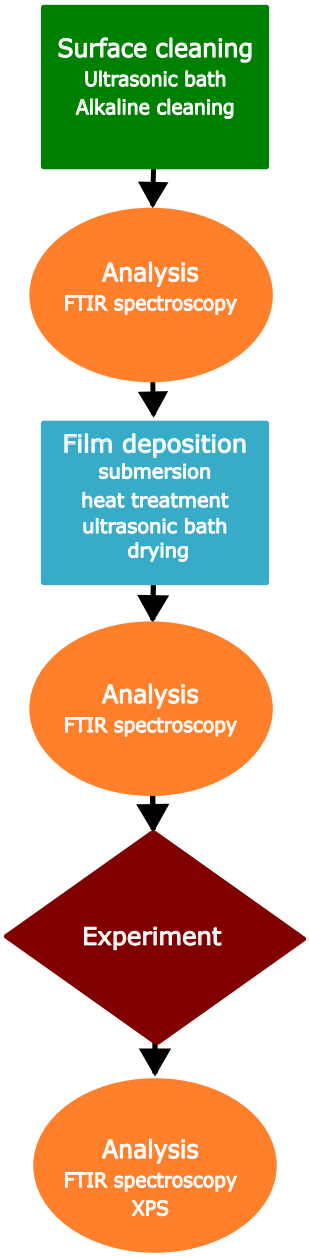

Figure 3.6: Flowchart of experimental procedure used in this study. Samples were analyzed in FTIR before and between every step of cleaning, film deposition and experiment execution. FTIR and XPS analysis were also conducted at the end of the experiment to obtain a final sample characterisation.

3.3 Preparation and deposition of thin film

The literature was consulted for a guide on preparing and depositing the SAMs. There are several different ways of applying a thin film on a metal substrate [44]. Growth from solution is the traditional route for the preparation of SAMs and was chosen for this study. This is a procedure where the metal substrate is submerged into a container where the depositing compound is mixed

with a suitable solvent. In this study, three different organic solvents were explored for each of the three SAMs. The organic solvents used were ethanol (C_2H_5OH), isopropanol (C_3H_8O), and toluene (C_7H_8).

3.3.1 Octadecyltrimethoxysilane (ODTMS)

Octadecyltrimethoxysilane (95%) with CAS-number 3069-42-9 was supplied by VWR International. A solution of 100 ml with 0.001 M ODTMS in ethanol was prepared in the following way: 5.6 ml of ODTMS was added to 90 ml of ethanol. The solution was adjusted to pH 4 by adding 3 ml acetic acid 98%. The solution was stirred for 3 h prior to the coating application on steel substrates [54].

A solution of ODTMS was prepared for the second solvent, isopropanol. Here, a solution of 100 ml with 0.001 M ODTMS in isopropanol was prepared in the following way: 5.6 ml of ODTMS was added to 90 ml of isopropanol. The solution was adjusted to pH 4 by adding 3 ml acetic acid 98%. The solution was stirred for 3 h prior to the coating application on steel substrates.

Lastly, a solution of 100 ml with 0.001 M ODTMS in toluene was prepared in the following way: 5.6 ml of ODTMS was added to 90 ml of toluene. The solution was adjusted to pH 4 by adding 3 ml acetic acid 98%. The solution was stirred for 3 h prior to the coating application on steel substrates.

3.3.2 Octadeclphosphonic acid (ODPA)

Octadeclphosphonic acid 98% with CAS number 4724-47-4 was supplied by VWR International. A solution of 100 ml with 0.001 M ODPA in isopropanol was prepared in the following way: 0.35 g of ODPA was added to 100 ml of isopropanol. The solution was stirred for 15 min and heated to 40 °C until all ODPA had gone into solution. The same procedure was repeated with ethanol and toluene as solvents [46] [65] [66] [45].

3.3.3 Stearic acid (SA)

Octadeclphosphonic acid 98% with CAS number 4724-47-4 was supplied by VWR International. A solution of 100 ml with 0.001 M ODPA in isopropanol was prepared in the following way: 0.25 g of ODPA was added to 100 ml of isopropanol. The solution was stirred for 15 minutes and heated to 40 °C until all SA had gone into solution. The same procedure was repeated with ethanol and toluene as solvents.

3.3.4 Coating procedure

The coating procedure for the steel samples are summarized in Table 3.2. The same procedure was followed for all samples, but the three different SAMs were found to have some differences in the literature. The difference lay in sample submersion time, as well as duration and temperature of heat treatment. ODTMS coated samples were submerged for 15 minutes for the deposition, and the heat treatment was conducted for 1 hour at 120 °C. ODPA coated samples were submerged for 8 hours for the deposition, and the heat treatment was conducted for 1 hour at 120 °C. Finally,

SA-coated samples were submerged for 20 hours for the deposition, and the heat treatment was conducted for 1 hour at 50 °C.

Table 3.2: Detailed, step wise representation of experimental procedure on steel samples.

Step	Procedure	Duration
1	Ultrasonic bath in ethanol	15 min
2	Alkaline cleaning in 2.5 M NaOH at room temperature	2 min
3	FTIR spectroscopy	-
4	Submersion in SAM solution	Variant dependent
5	Heat treatment in oven at variant dependent temperature	Variant dependent
6	Cooling	10 min
7	Ultrasonic bath in isopropanol	1 min
8	Ultrasonic bath in deionized water	1 min
9	Blow drying with air gun	20 sec
10	FTIR spectroscopy	-
11	Experiment	4 weeks
12	FTIR spectroscopy	-
13	XPS	-

3.3.5 Scratchplate from electric guitar

An experiment was conducted to model the corrosion on steel in contact with an item known to contain actively degrading cellulose nitrate. Steel samples were put in contact with a museum artefact from the Rockheim collection, the scratchplate from an electric guitar (museum id. Rock 2725) (Figure 3.7, for four weeks. The samples were cleaned in 2.5 M NaOH at room temperature for 2 min prior to the exposure. The samples were investigated in FTIR before and after the experiment. XPS was also conducted after the finished experiment.

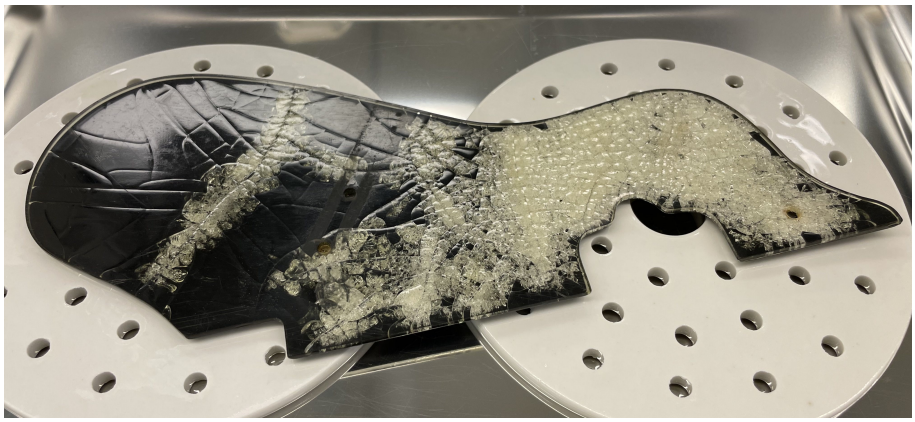

Figure 3.7: Scratchplate taken from electric guitar in the Ringve collection. Museum id. : Rock 2725

Another experiment was conducted on the same object, where steel samples were coated with the three different thin films, ODPA, ODTMS, and SA. The samples were then exposed to the cellulose nitrate scratchplate the same way as the ones with the uncoated steel. In this experiment, the organic thin films were synthesized using two different types of organic solvents, namely ethanol

and toluene. The samples were left in contact for four weeks. The samples were investigated in FTIR before and after the experiment. XPS was also conducted after the finished experiment. Table 3.3 summarizes the difference in sample pre-treatment for the experiment.

Table 3.3: Step wise representation of pre-treatment on steel samples exposed to scratchplate

Sample ID	**Sample pre-treatment**
Fe G1	Alkaline cleaning
ODPA-ethanol	Ultrasonication in ethanol for 15 min, Alkaline cleaning in 2.5 M NaOH at room temperature for 2 min, dipped for 8 hours in a solution of ODPA in ethanol, heat-treated at 120 °C for 1 h.
SA- toluene	Ultrasonication in ethanol for 15 min, Alkaline cleaning in 2.5 M NaOH at room temperature for 2 min, dipped for 20 hours in a solution of SA in toluene, heat-treated at 50 °C for 3 h.
SA-ethanol	Ultrasonication in ethanol for 15 min, Alkaline cleaning in 2.5 M NaOH at room temperature for 2 min, dipped for 20 hours in a solution of SA in ethanol, heat-treated at 50 °C for 3 h.
ODTMS- toluene	Ultrasonication in ethanol for 15 min, Alkaline cleaning in 2.5 M NaOH at room temperature for 2 min, dipped for 1 hour in a solution of ODTMS in toluene, heat-treated at 120 °C for 1 h.

3.3.6 Cellulos nitrate from accordion

A similar experiment was conducted where steel samples were placed in contact with the cellulose nitrate plate from an accordion for four weeks (figure 3.8). The samples were cleaned in 2.5 M NaOH at room temperature for 2 min prior to the exposure. The samples were investigated in FTIR before and after the experiment. XPS was also conducted after the finished experiment.

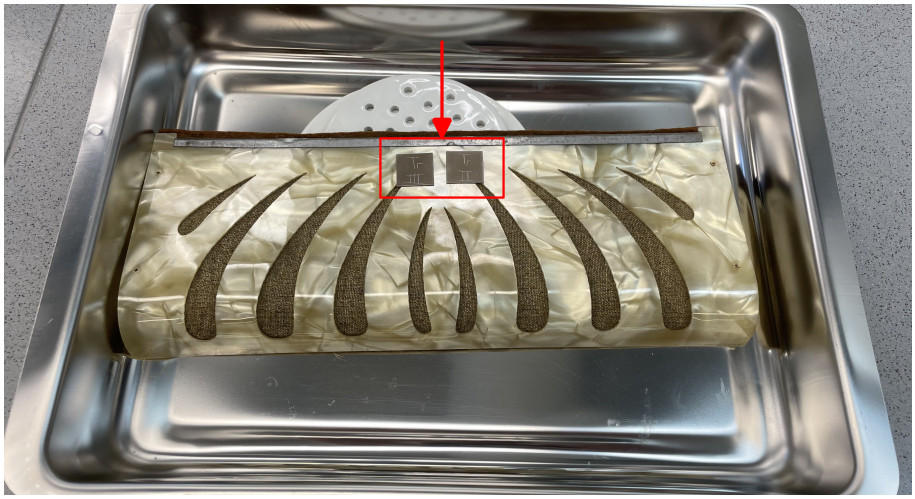

Figure 3.8: Cellulose plate taken from the grill of an accordion. The red square indicates the placement of steel samples during the experiment.

3.3.7 Surface finish

An experiment was conducted were different surface cleaning procedures were investigated. Steel samples were cleaned in alkaline solution and rinsed with deionized water, and subsequently subjected to rinsing with either ethanol, isopropanol or acetone. The samples were then examined in FTIR. The treatment procedure for each sample is presented in table 3.4.

Table 3.4: Step wise representation of the experimental procedure for surface finish experiment.

Step	Sample	treatment
1	All	Cleaning in 2.5 M NaOH for 2 min
2	All	Rinsing with deionized water
3	Feacetone	Rinsing with acetone
	Feethanol	Rinsing with ethanol
	Feisopropanol	Rinsing with Isopropanol
4	All	Drying with air gun
5	All	FTIR spectroscopy

3.4 Diphenylamine spot test

A solution of 0.5% diphenylamine in 90% sulfuric acid was prepared in the following way: 90 ml of concentrated sulfuric acid was slowly added to 10 ml of water while stirring continuously. This was added in small portions to 0.5 g of diphenylamine, resulting in a clear, transparent reagent solution.

The spot test was conducted in the following way: A tiny chip of material was taken from an unobtrusive part of the object to be tested. No more than a pinhead is a sufficient amount of material for a successful test. The sample was placed on a glass surface. A single drop of reagent was placed on the sample using a pipette, and the development of the visual characteristics of the drop was examined. The indication of the presence of cellulose nitrate would be characterized by a transition in the drop from transparent to a blue-violet stain within seconds in contact with the sample. No color change or the appearance of other colors would indicate that cellulose nitrate is absent.

3.5 Analysis

3.5.1 FT-IR

The FT-IR spectra were recorded with a VERTEX 80v vacuum spectrometer manufactured by Bruker Optics (Ettlingen, Germany), used in transmission mode in the 400–4000 cm^{-1} range. 100 scans with a resolution of 4 cm^{-1} were acquired for each FTIR spectrum. The samples were either steel or plastic material, as specified in the reported results.

FTIR with grazing incidence was done on the steel. The reference was a steel sample freshly cleaned in 2.5 M NaOH (The same as the starting point for all samples). The respective samples were baseline corrected using the built-in algorithm of the Bruker OPUS software.

FTIR ATR was used on the cellulose nitrate from the musical instruments with a platinum diamond sampling accessory.

3.5.2 Raman spectroscopy

Raman spectroscopy measurements were performed with an Alpha300 R manufactured by Witec (ulm, Germany) using the 523 nm wavelength incident light of a frequency-doubled-solid-state Nd-YAG laser. Laser power was set to 66 mW. Integration time was set to 180 seconds.

3.5.3 XPS

XPS analysis was performed by Verner Håkonsen at the department of nanotechnology at NTNU. Measurements were done with an Axis Ultra DLD machine manufactured by Kratos Analytical. The photoelectrons were exited using a monochromatic Al-Kα source. X-rays beam were generated with 15mA and 12 kV in the filament. The pressure in the analysis chamber was kept below 10^{-8} Torr. Acquisition parameters for the individual measurements are tabulated in appendix A

The spectra were treated with the CasaXPS software. A Shirley background was employed for the quantification of spectra. The quantification was done with curve fitting within the software.

3.5.4 Identification of samples

For the purpose of practicality, a sample naming system was devised for the steel samples as shown in table 3.5. These names may recur in figures and tables throughout the results. The first letters indicate what type of compound the coating is made of, either ODTMS, ODPA, SA or U (uncoated). The next letters denote what type of solvent has been used to make the coating, or the location in which the sample were placed. "L" meaning "Lab", and "D" meaning "Dora" (which is the storage facility of the museum). The names were engraved into the top surface of the respective samples to avoid any mix ups.

Table 3.5: Explanatory table for sample identification of the steel samples.

Sample ID	**Description**			
	Coating	**Solvent**	**Contact**	**location**
ODPA-D	ODPA	Isopropanol	White cotton	Dora
ODTMS-D	ODTMS	Isopropanol	White cotton	Dora
SA-D	SA	Isopropanol	White cotton	Dora
U-D	Uncoated		White cotton	Dora
ODPA-L	ODPA	Isopropanol	White cotton	Lab
ODTMS-L	ODTMS	Isopropanol	White cotton	Lab
SA-L	SA	Isopropanol	White cotton	Lab
U-L	Uncoated		White cotton	Lab
ODPA-RL		Isopropanol	Red felt	Lab
ODTMS-RL	ODTMS	Isopropanol	Red felt	Lab
SA-RL	SA	Isopropanol	Red felt	Lab
U-RL	Uncoated		Red felt	Lab
G1			Guitar scratchplate	lab
A1			Accordion	lab

4 Results

This section is dedicated to presenting the most significant experimental results obtained in this study. This includes FTIR- and XPS-spectra data, Raman spectra, images of corrosion phenomena, and results from the conducted diphenylamine spot test.

4.1 Fourier transfrom infrared spectroscopy (FTIR)

4.1.1 Grazing incidence (GI)

Steel samples were analyzed in FTIR spectroscopy with grazing incidence. The spectra were recorded using a KBr beam splitter. The reference was a cleaned steel sample. Figure 4.1 shows the IR-spectra of a steel sample after cleaning, dip-coating with ODPA from an isopropanol solution, and exposed to cotton fabric inside the instrument casing for four weeks. The characteristic peaks are summarized in table 4.1.

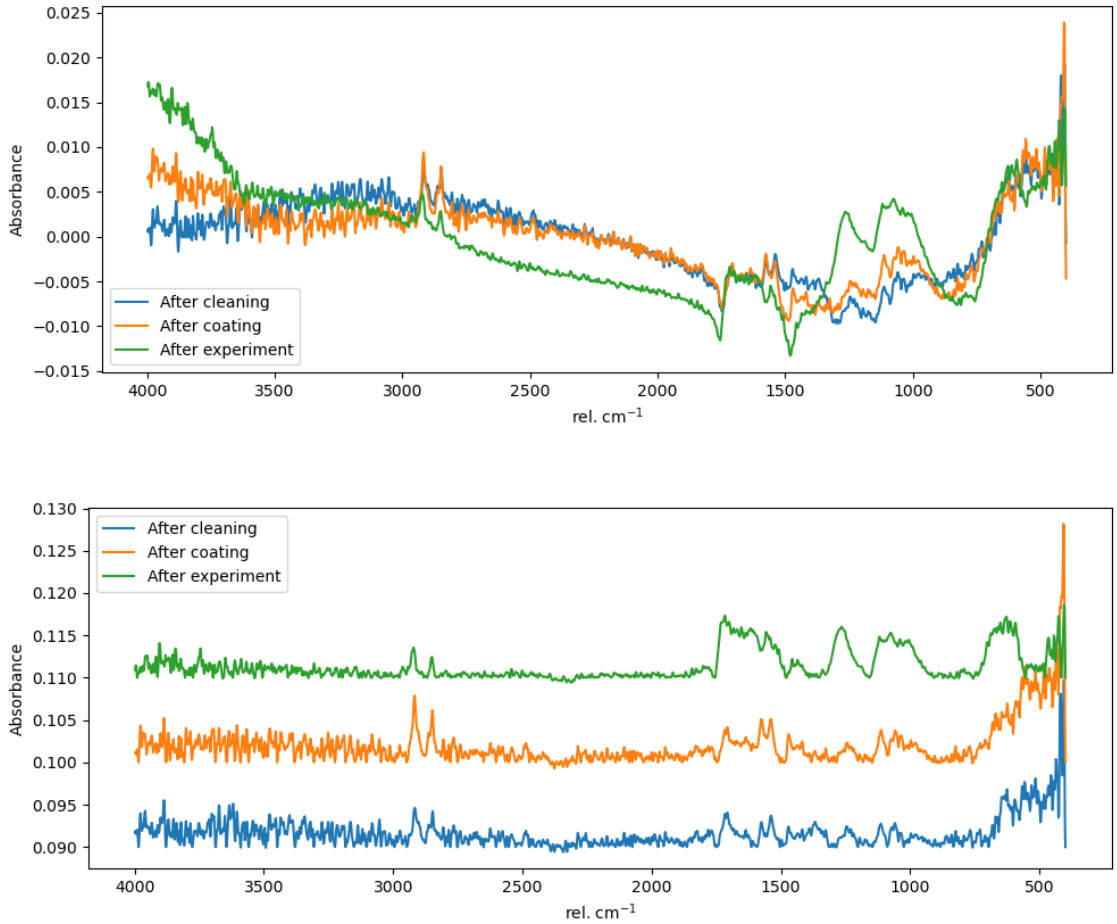

Figure 4.1: FTIR spectrum for steel sample coated with ODPA after cleaning, after coating and after experiment. Raw spectra (top) and baseline corrected (bottom).

Figure 4.2 shows the IR-spectra of a steel sample after cleaning, dip-coating width ODTMS from an isopropanol solution, and exposed to cotton fabric inside the instrument casing for four weeks.

Figure 4.2: FTIR spectrum for steel sample coated with ODTMS After cleaning, after coating, and after the experiment. Raw spectra (top) and baseline corrected (bottom).

Figure 4.3 shows the IR-spectra of a steel sample after cleaning, dip-coating width SA from an isopropanol solution, and exposed to cotton fabric inside the instrument casing for four weeks.

Figure 4.3: FTIR spectrum for steel sample coated with SA After cleaning, after coating, and after the experiment. Raw spectra (top) and baseline corrected (bottom).

Figure 4.4 shows the IR-spectra of a steel sample after cleaning, and after exposed to cotton fabric inside the instrument casing for four weeks.

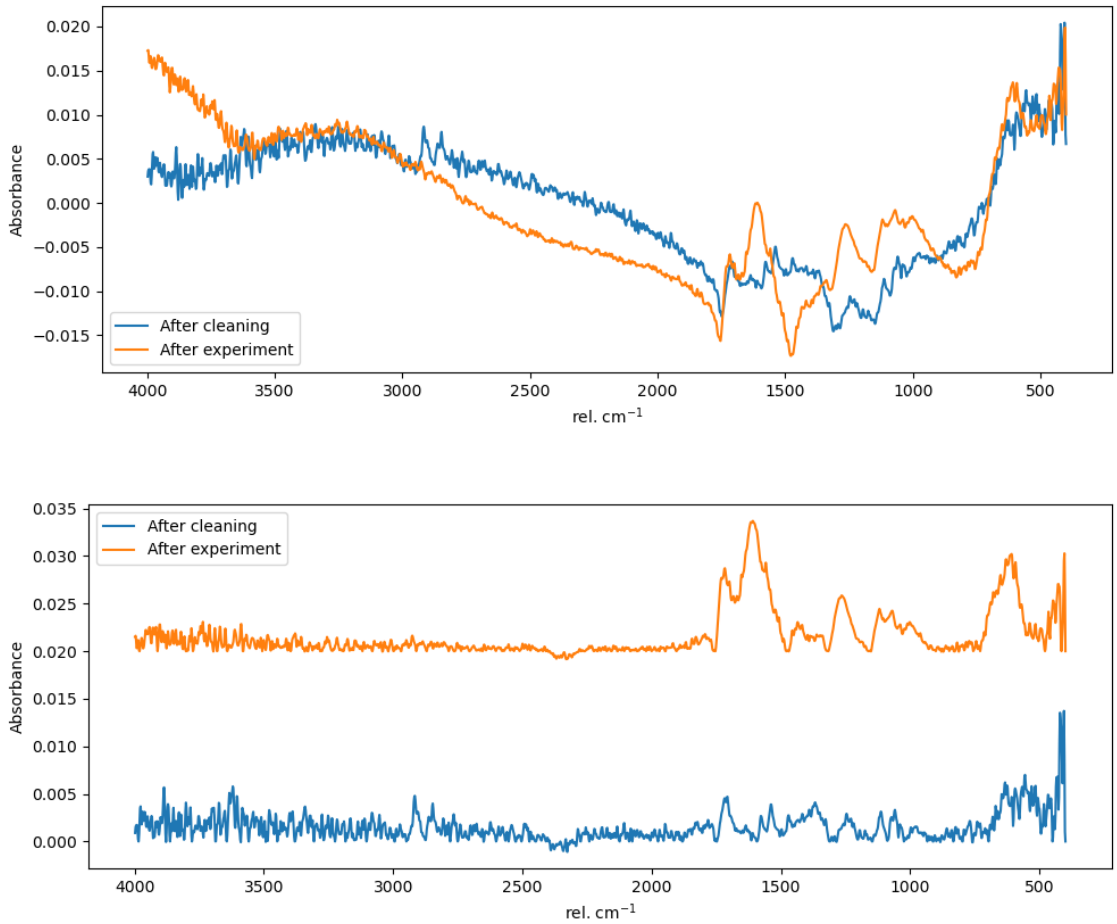

Figure 4.4: FTIR spectrum for uncoated steel sample after cleaning, and after the experiment. Raw spectra (top) and baseline corrected (bottom).

Figure 4.5 compares the IR-spectra of the steel samples of the uncoated sample, ODPA, SA, and ODTMS, after exposure to cotton fabric inside the instrument casing for four weeks. Table 4.1 summarize the characteristic peaks for the spectra.

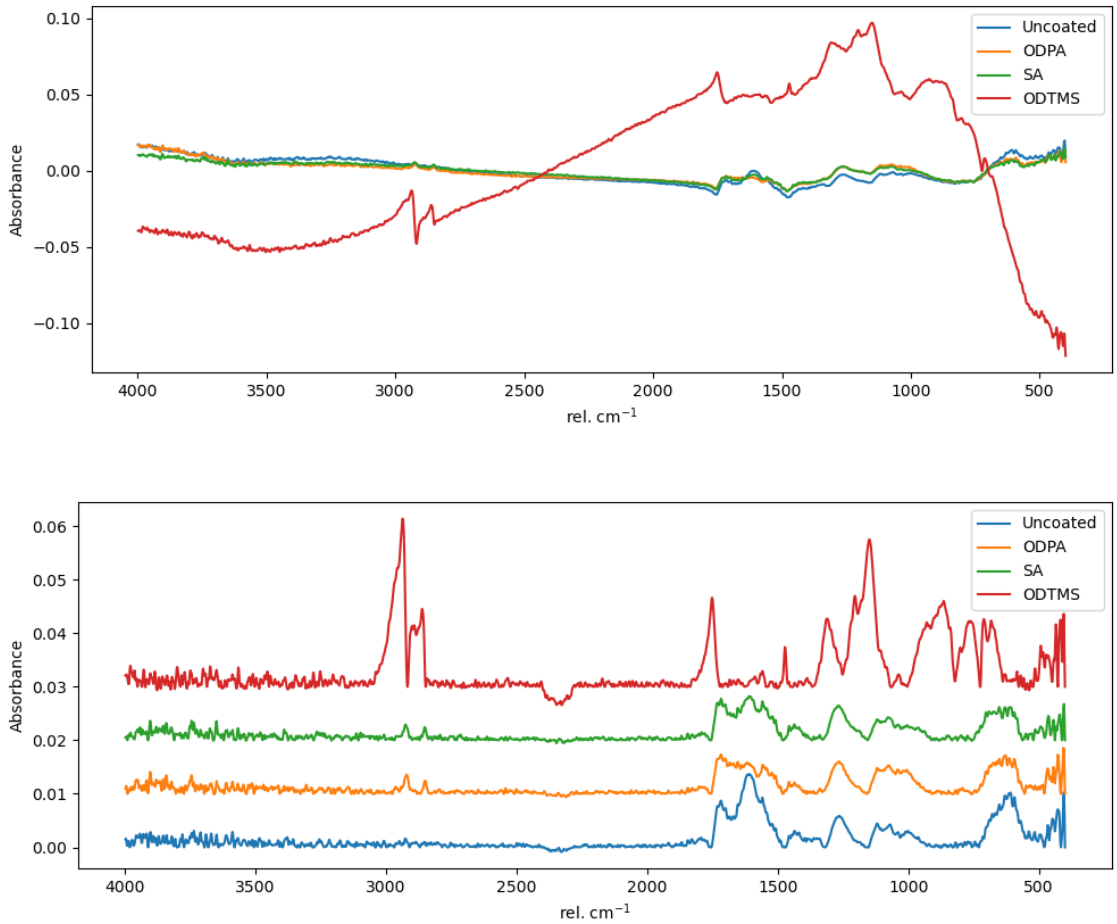

Figure 4.5: FTIR spectrum comparison of uncoated sample, SA, ODPA and ODTMS after four weeks of contact with cotton fabric. Raw spectra (top) and baseline corrected (bottom).

Table 4.1: Characteristic peaks of FTIR spectra for steel coated with ODTMS, ODPA and SA from an isopropanol solution, and an uncoated sample. All were exposed to cotton fabric inside the instrument casing for four weeks.

Sample	**Wavenumber [rel.cm^{-1}]**													
ODTMS	2935	2896	2859	1751	1558	1472	1309	1205	1148	930	865	766	711	682
SA	2922	2850	1732	1609	1558	1458	1263	1119	633					
ODPA	2922	2850	1732		1558	1458	1263	1119	633					
Uncoated			1732	1609	1558	1458	1263	1119	633					

In this study, three types of organic solvents were tested for the dip-coating process of the coating systems. The following presents the IR-spectra of the samples after coating deposition, heat treatment, and cleaning of excess solvent. All spectra were measured against a cleaned steel sample as a reference.

The synthesis of ODPA in a toluene solution was unsuccessful. Therefore figure 4.6 shows the IR-spectra of ODPA-coated steel samples from isopropanol and ethanol solutions. Both coatings seem to affect the substrate. The Two peaks at 2922 and 2850 suggest the presence of several CH2-group chains [67, 68]. They are most prevalent for ODPA coated from an ethanol solution.

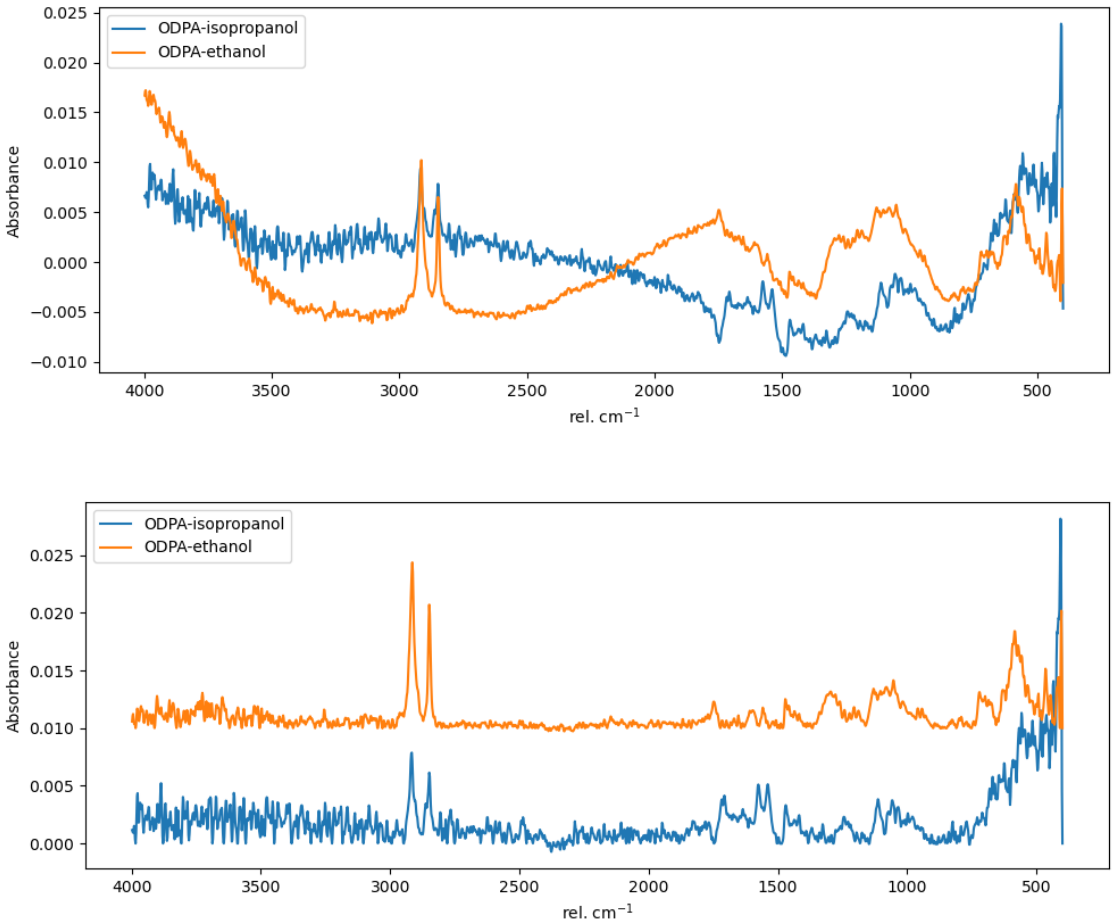

Figure 4.6: FTIR spectrum comparison of ODPA-coated samples from a solution of isopropanol or ethanol. Raw spectra (top) and baseline corrected (bottom).

The synthesis of ODTMS in an ethanol solution was unsuccessful. Therefore figure 4.6 shows the IR-spectra of ODTMS-coated steel samples from isopropanol and toluene solutions only. It can be seen that the ODTMS-isopropanol solution has a more significant effect on the steel.

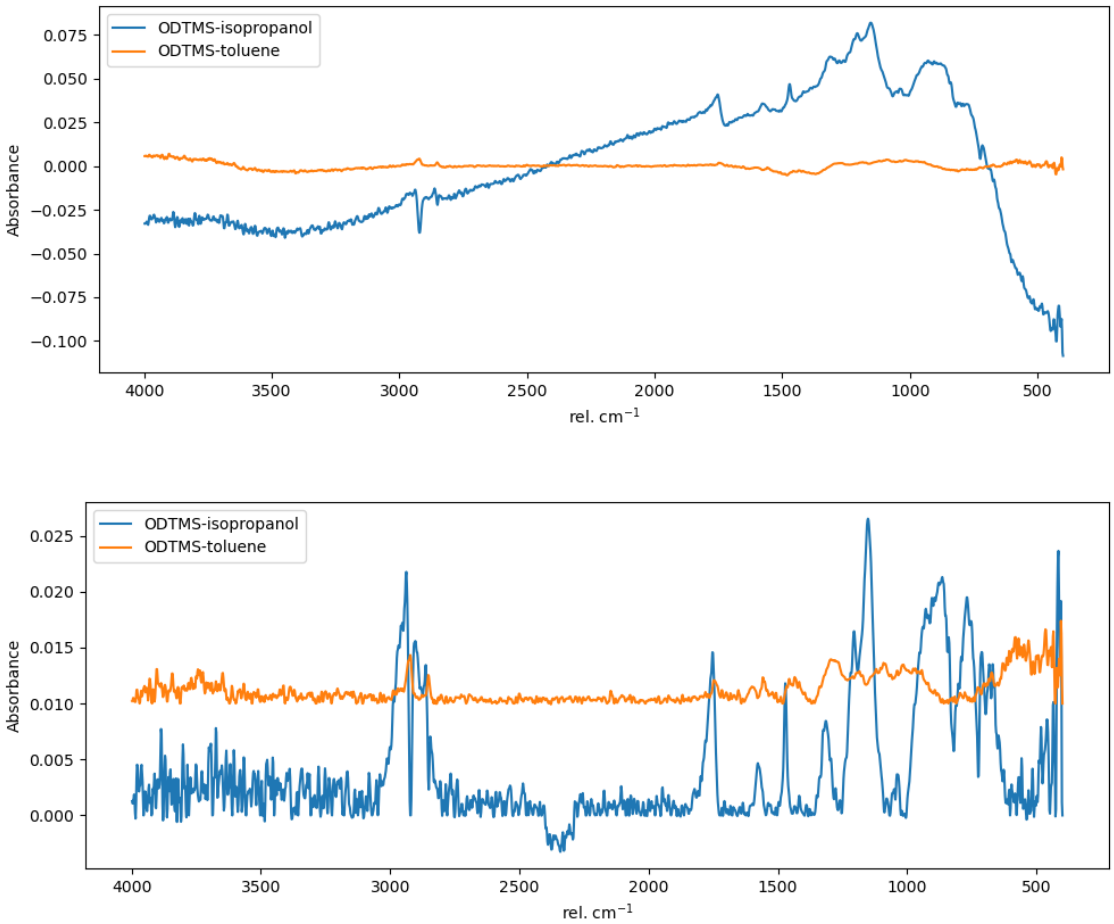

Figure 4.7: FTIR spectrum comparison of ODTMS-coated samples from a solution of isopropanol or toluene. Raw spectra (top) and baseline corrected (bottom).

Figure 4.6 shows the IR-spectra of SA-coated steel samples from isopropanol, ethanol and toluene solutions.

Figure 4.8: FTIR spectrum comparison of SA-coated samples from a solution of isopropanol, ethanol or toluene. Raw spectra (top) and baseline corrected (bottom).

4.1.2 Surface finish

Three steel samples were subjected to cleaning with different surface finishing, either with ethanol, acetone or isopropanol. Figure 4.9 shows the resulting IR-spectrum of the different samples at lower wavenumbers. A mylar beam splitter was used, and the spectra were measured against a steel cleaned steel reference with a deionized water finish.

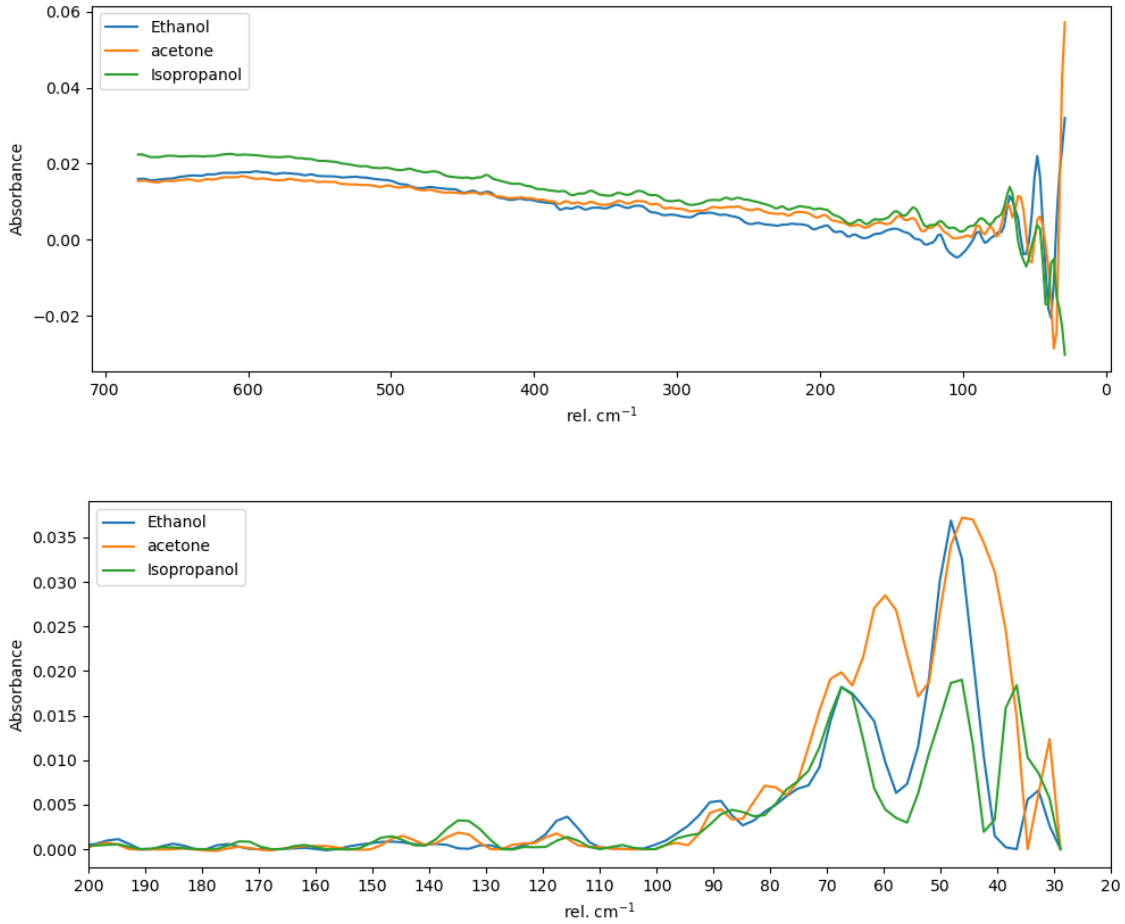

Figure 4.9: FTIR spectrum comparison of the steel samples cleaned in alkaline solution and rinsed with deionized water, and subsequently subjected to rinsing with either ethanol, isopropanol or acetone. Raw spectra (top) and baseline corrected spectrum at lower wavenumbers (bottom).

Table 4.2: Characteristic peaks of FTIR spectra of steel samples subjected to rinsing with either ethanol, acetone or isopropanol,

Sample	**Wavenumber [rel.cm^{-1}]**						
Ethanol		115	89		67	47	32
Acetone	134		89	80	67	45	30
Isopropanol	134	89			67	47	37

4.1.3 Attenuated total reflectance (ATR)

A sample from each of the four instruments, electric guitar (Rock 2725), Mandolin-banjo (RMT 721), accordion, and surbahar (RMT 66/23) was subjected to FTIR spectroscopy with attenuated total reflectance. Two of these, the guitar and the accordion, were already known to contain cellulose nitrate. The IR-spectrum of the respective samples is presented in figure 4.10 and important characteristics are summarized in table 4.3

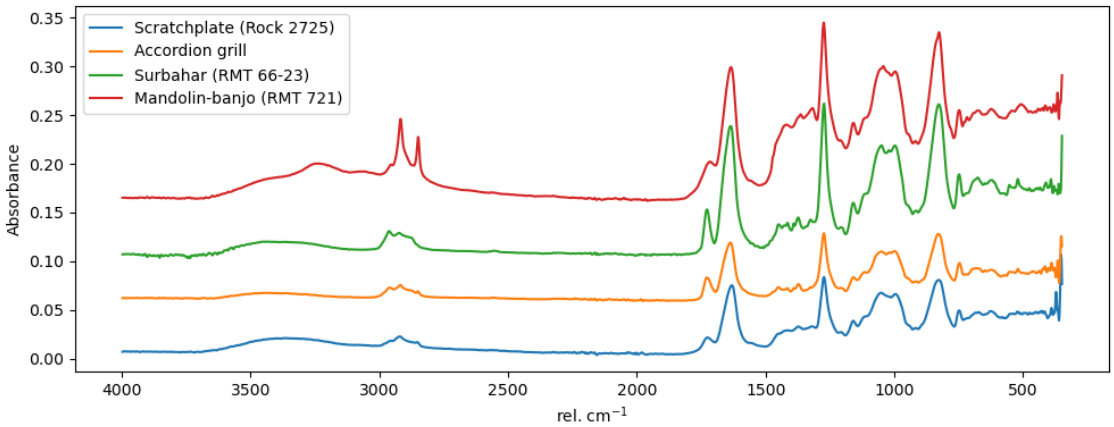

Figure 4.10: FTIR-spectra of sampled material from four different instruments. An obvious similarity in peak positions can be seen.

Table 4.3: Assignments of main infrared absorption bands of instrument samples [5].

Wavenumber (cm^{-1})	**Assignment**
3500	ν OH
2965	ν_a CH in $-CH_2-$ in cellulosic backbone
2905	ν_s CH in $-CH_2-$ in cellulosic backbone
1730	ν_s C=O of ketone
1650	ν_a NO2
1460	δ CH2 in cellulosic backbone
1375	δ CH in cellulosic backbone
1280	ν_s NO2
1160	$C_5OC_1OC_4$ (acetal structure of polysaccharides)
840	ν NO
750	δ NO2

ν_s = symmetric strench, ν_a = asymmestric stretch, δ = scissoring

4.2 X-ray photoelectron spectroscopy (XPS)

4.2.1 Cleaned and coated samples

After FTIR, the steel samples were analyzed using X-ray photoelectron spectroscopy. A survey spectrum was obtained to identify elements present at the top 1-3 nanometers of the surface. Figure 4.11 shows the survey spectrum for a reference steel sample and three coated samples, each with one of the three proposed coating systems. All XPS-spectra were charge corrected, which means the binding energy was calibrated such that the aliphatic component in the carbon 1s peak is at 285 eV.

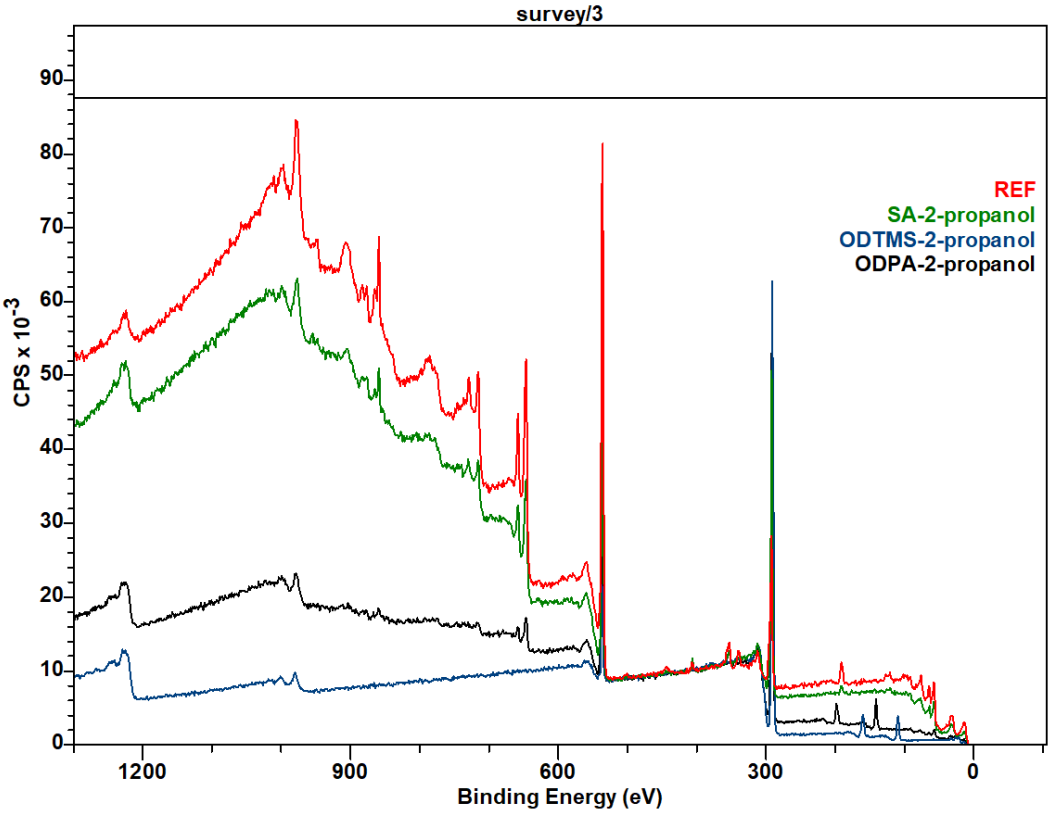

Figure 4.11: Survey scan comparing the three types of coated surfaces (ODPA, ODTMS and SA) after dip-coating in a 2-propanol solution, and a cleaned steel reference.

Elemental quantification was done on the samples from the survey scan. Figure 4.12 shows the elemental quantification of the steel reference sample after ultrasonic bath and alkaline cleaning. The results from the quantification of the coated samples are summarized in table 4.4. Included in table 4.4 are also elemental quantification of samples coated from ethanol and toluene solutions.

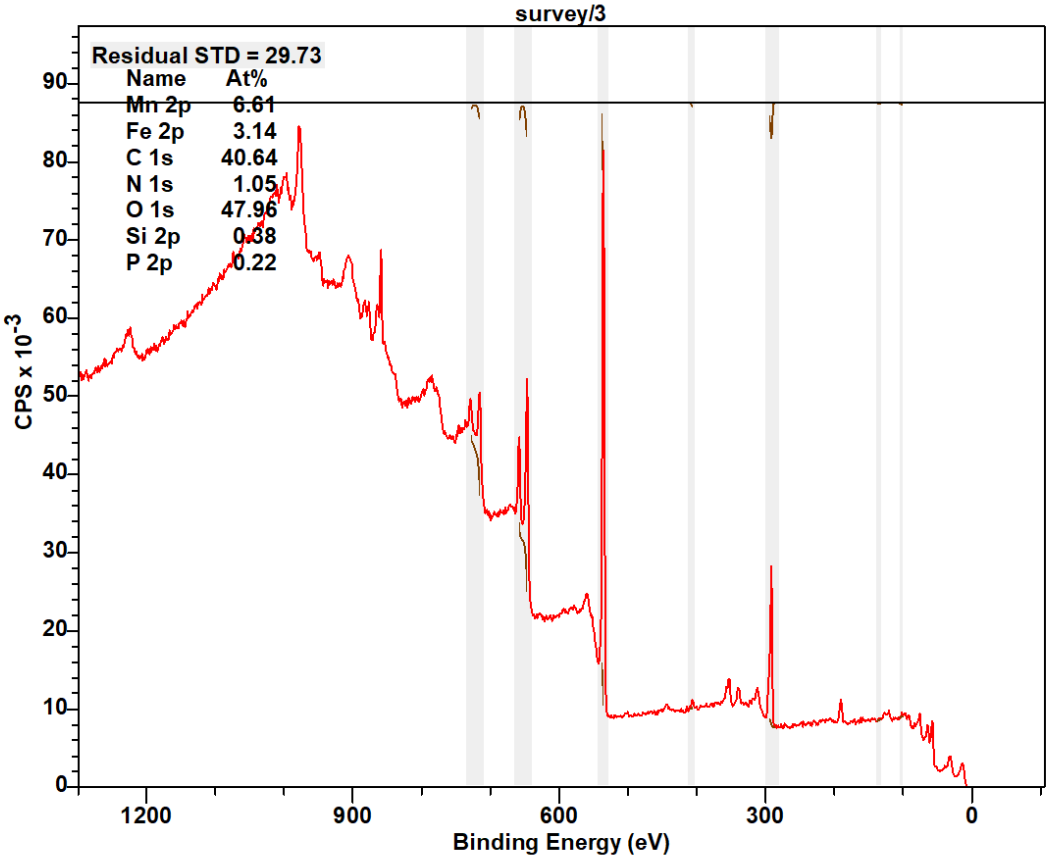

Figure 4.12: Elemental quantification in atomic percent from survey scan of reference sample.

Table 4.4: Quantification from survey spectra in atomic percent from coated samples from an isopropanol solution and samples coated from ethanol and toluene solutions.

Sample	Element (at%)						
	C	O	Fe	Mn	P	Si	N
REF	60.64	47.96	3.14	6.61	0.22	0.38	1.05
ODPA-2-propanol	80.76	13.04	0.15	0.71	5.33		
ODTMS-2-propanol	87.92	6.85				5.22	
SA-2-propanol	69.44	26.19	0.73	2.14			1.51
ODPA-ethanol	71.15	23.53	0.48	1.74	3.11		
ODTMS-toluene	67.15	25.87	0.60	1.53		3.44	1.42
SA-ethanol	73.15	24.11	0.61	1.48			
SA-toluene	71.42	24.94	0.48	1.60			0.55

A high-resolution XPS spectrum was recorded for all samples of the carbon 1s peak. The spectrum was peak fitted with the assumption that it contains contributions from four different classes of carbon bonds: aliphatic (C-C, C-H), alcohol and ether (C-OH, C-O-C), and ketones (C=O), esters and acids (O-C=O). Figures 4.13-4.16 shows the peak fit for each sample. The calculation from this fit provides a quantification of the different components. The line shapes of the peaks are clearly different between the four samples.

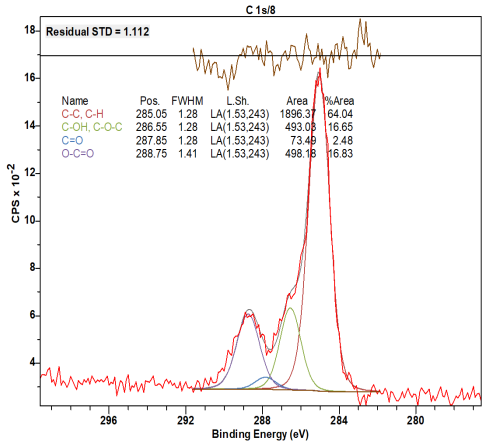

Figure 4.13: High resolution XPS spectrum for the carbon 1s peak for reference sample. The spectrum is assumed to comprise of 4 different bonding types.

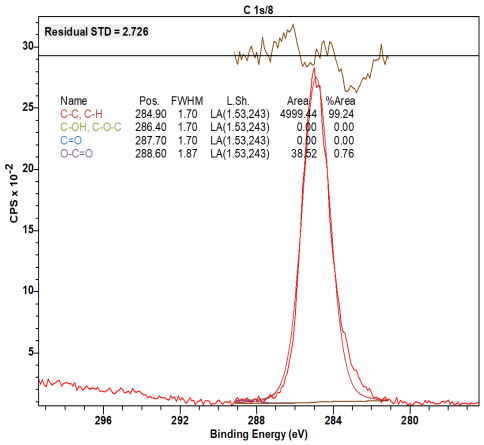

Figure 4.14: High resolution XPS spectrum for the carbon 1s peak for ODPA-2-propanol.

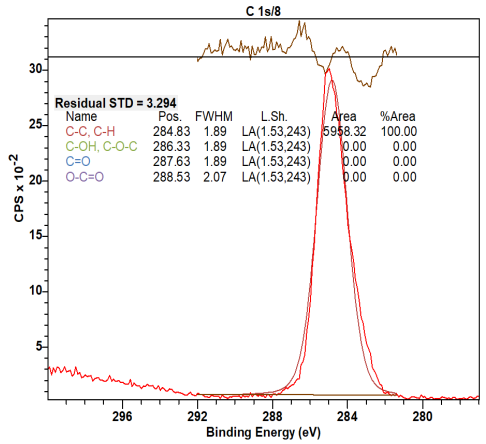

Figure 4.15: High resolution XPS spectrum for the carbon 1s peak for ODTMS-2-propanol.

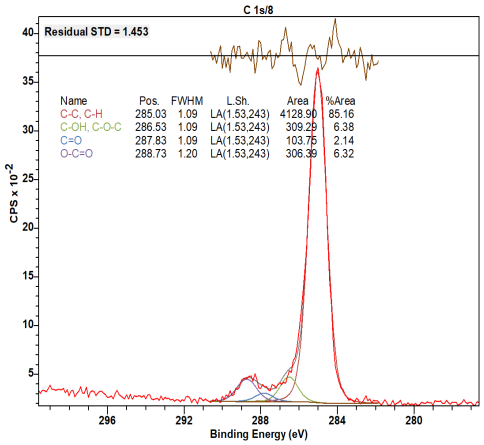

Figure 4.16: High resolution XPS spectrum for the carbon 1s peak for SA-2-propanol.

The quantification of bonding mode for the reference and the three coated samples of the C1s peak is summarized in table 4.5. The quantification reveals that the aliphatic component is prevalent in all three coated samples. ODTMS and ODPA appear to have no other contributing components indicating a thick layer of aliphatics. SA shows the same tendency but to a lower degree.

Table 4.5: Quantification of bonding types for the carbon 1s peak of the measured steel samples in area%.

Sample	**Bonding type (area %)**			
	C-C, C-H	**C-OH, C-O-C**	**C=O**	**O-C=O**
REF	64.04	16.65	2.48	16.86
ODPA-2-propanol	99.24			0.76
ODTMS-2-propanol	100.00			
SA-2-propanol	85.16	6.38	2.14	6.32

4.2.2 Steel samples exposed to textile

Four samples were exposed to white cotton fabric inside the square piano at the storage facility. Four samples were exposed to white cotton fabric, and four to red wool felt inside a desiccator with controlled humidity. The samples were analyzed with XPS after the experiment was concluded. All samples were subject to elemental quantification, and the results are summarized in table 4.6. The survey scans for each sample can be found in appendix A.

Table 4.6: Quantification from survey spectra in atomic percent from the samples contained in contact with textile fabric.

Sample	**Element (at%)**									
	C	**O**	**Fe**	**Mn**	**P**	**Si**	**N**	**Ca**	**Na**	**Al**
REF	60.64	47.96	3.14	6.61	0.22	0.38	1.05			
ODPA-D	70.52	25.38	0.55	1.26	2.23	0.07	0			
ODPA-L	68.72	26.10	0.85	1.83	2.50	0	0			
ODPA-RL	72.49	21.56	0.43	1.28	4.25	0	0			
ODTMS-D	86.67	8.16				5.15				
ODTMS-L	87.36	7.06				5.58				
ODTMS-RL	85.42					5.64				
SA-D	70.25	26.76	0.92	2.07						
SA-L	71.07	26.14	0.90	1.89						
SA-RL	72.75	25.28	0.62	1.34						
U-D	38.38	47.93	3.33	8.51		0.33	0.48			
U-L	59.56	38.62	2.29	5.09			2.58	0.87		
U-RL	41.81	43.85	3.02	5.93			2.47		1.03	1.89

Table 4.7 summarize the peak fit for the carbon 1s peak for all steel samples in the experiment. It can be seen that there is variation in the prevalent bonding type between coating types and relative to the uncoated samples as well as the refernce. Coated samples appear to have higher percentage of the aliphatic bonding types, and ODTMS coated samples seem to be completely dominated by this. The graphs of the peak fit for each sample is found in appendix A.2

Table 4.7: Quantification of bonding types for the carbon 1s peak of the measured steel samples in area%.

Sample	Bonding type (area %)			
	C-C, C-H	**C-OH, C-O-C**	**C=O**	**O-C=O**
REF	64.04	16.65	2.48	16.86
ODPA-D	68.03	18.86	6.03	7.09
ODPA-L	88.20	6.98	0.88	3.94
ODPA-RL	73.83	13.56	9.55	3.06
ODTMS-D	100	0	0	0
ODTMS-L	100	0	0	0
ODTMS-RL	99.13	0	0.87	0
SA-D	81.63	9.08	2.83	6.46
SA-L	84.06	8.85	1.76	5.33
SA-RL	71.72	16.44	4.11	7.73
U-D	65.55	12.30	3.61	18.53
U-L	69.10	15.22	4.24	11.43
U-RL	60.64	16.81	5.68	16.88

4.3 Raman spectroscopy

Raman spectroscopy was used in an attempt to record the gas that the actively deteriorating cellulose nitrate scratchplate releases. A spectrum of empty air was first recorded using maximum laser power (60mW) and an integration time of 3 minutes. The scratchplate was analyzed by focusing the laser on a point right above the surface to detect any gases. the resulting spectra are shown in figure 4.17. The recorded peaks are summarized in table 4.8.

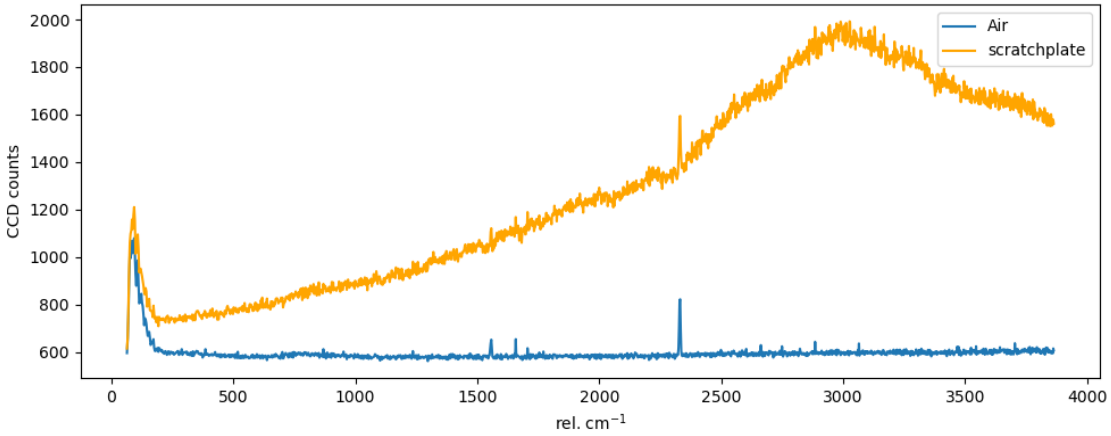

Figure 4.17: Raman spectra comparison between empty air (blue) and the air above cellulose nitrate scratchplate (orange).

Table 4.8: Characteristic peaks of the raman spectra of empty air and the air above cellulose nitrate scratchplate.

Sample	Wavenumber [rel.cm^{-1}]			
Air	1557	1658	2331	2884
Scratchplate	1557	1658	2331	2884

4.3.1 Diphenylamine spot test

The diphenylamine spot test was performed on two samples, known to contain cellulose nitrate, namely the electric guitar scratchplate (figure 4.19) and the accordion grill (figure 4.18). these served as a reference for examining the samples from the mandolin-banjo and the surbahar. All samples gave a positive indication of the presence of cellulose nitrate.

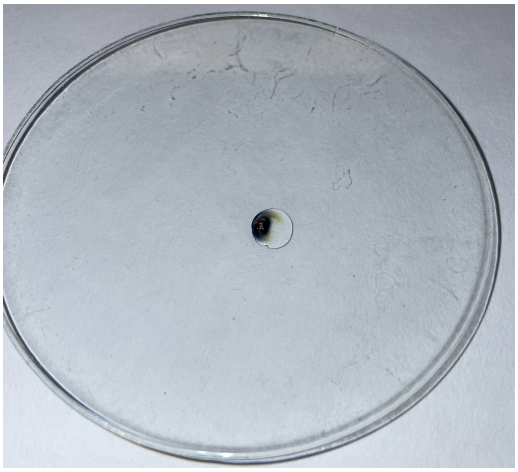

Figure 4.18: Diphenylamine spot test of sample material taken from the cellulose nitrate accordion-piece showing a dark blue color.

Figure 4.19: Diphenylamine spot test of sample material taken from the cellulose nitrate scratchplate showing a dark blue color.

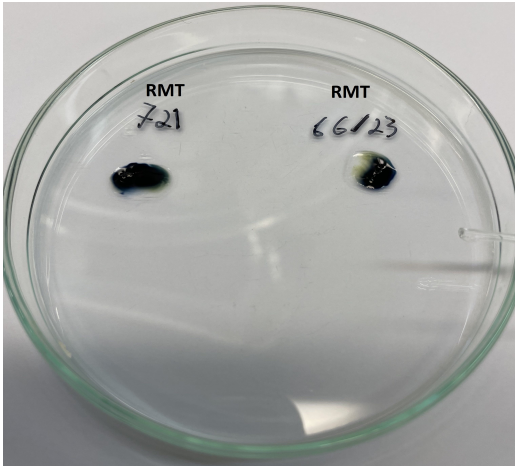

Figure 4.20: Diphenylamine spot test of sample taken from the mandolin-banjo (left) and surbahar (right). The drops formed a dark blue color which indicates the presence of cellulose nitrate.

4.4 Visual examination

Visual examination indicate that there are slight differences of corrosion on the various samples kept in contact with cellulose nitrate scratchplate in figures 4.21 and 4.22. The uncoated samples have experienced heavy corrosion and got a uniform brown color from iron oxide.

In the coated samples, there is a significant difference in the severity of corrosion attack. For the sample coated with SA from a toluene solution (no 1 in figure 4.22) and the sample coated with ODPA from a toluene solution (no. 3), the corrosion appears the same as for the samples without coating. ODTMS-isopropanol(no 4), ODPA-ethanol (no 5), and SA-ethanol (no 6) performed slightly better but only marginally. ODTMS from ethanol solution (no 2) performed noticeably better than the rest of the coated and uncoated samples. However, the coating also seems ineffective on large parts of this sample.

No sign of corrosion can be seen on samples that were in contact with the accordion grill, as shown in figure 4.23.

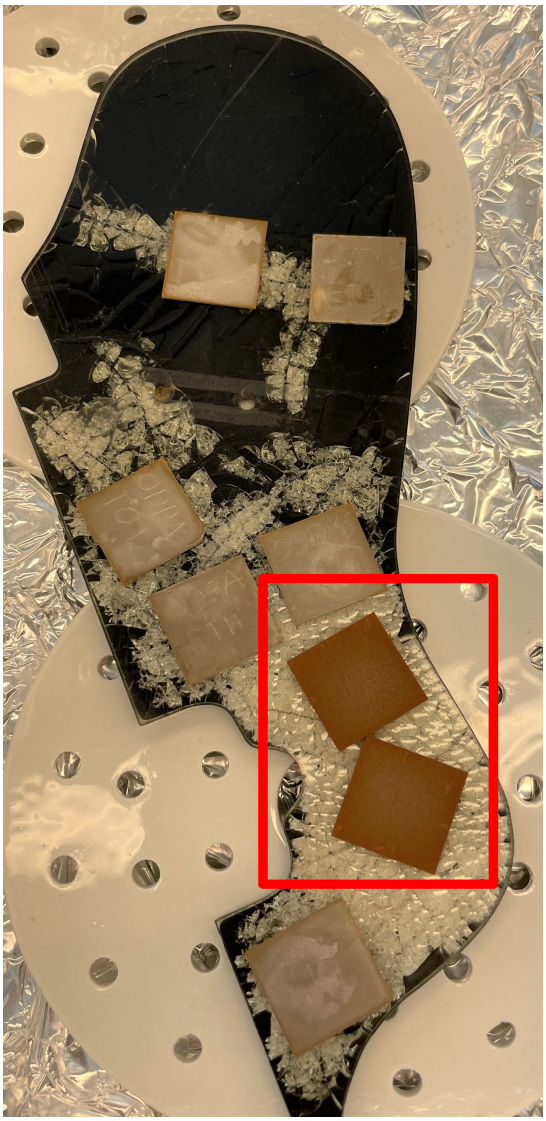

Figure 4.21: Uncoated steel samples after three weeks of exposure to scratchplate (marked with red).

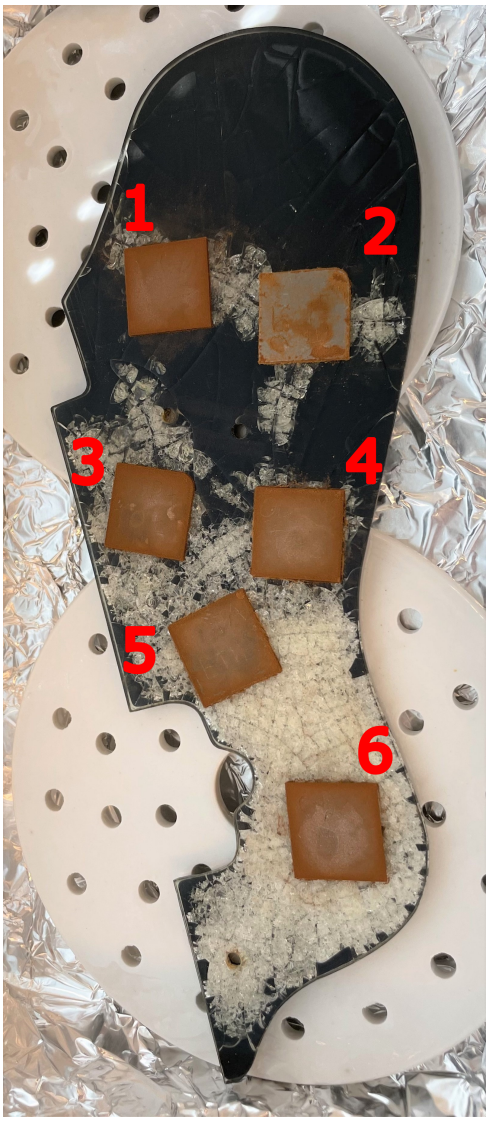

Figure 4.22: Coated steel samples after three weeks of exposure to scratchplate. SA-ethanol (1), ODTMS-isopropanol (2), ODPA-isopropanol (3), ODTMS-toluene (4), ODPA-ethanol (5), SA-ethanol (6)

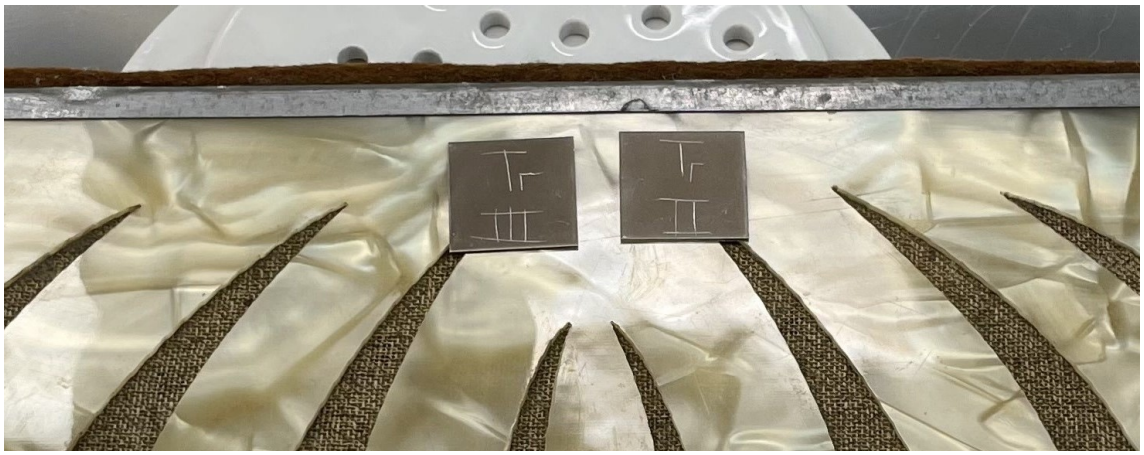

Figure 4.23: Uncoated steel samples after four weeks of contact with cellulose nitrate plate from an accordion.

An observation was made about the location of the first signs of corrosion. The steel corroded the most in places where the cellulose nitrate has cracked, as shown in figure 4.24.

Figure 4.24: SA-tol Steel sample after two weeks of contact with cellulose nitrate scratchplate. A line of corrosion goes across the sample which coincided with a large crack in the cellulose nitrate plate.

5 Discussion

5.1 Cellulose nitrate

Seeking confirmation on the material suspected of being responsible for corrosion on the mandolin-banjo (RMT 721) and the surbahar (RMT 66/23), a diphenylamine spot test was conducted, which gave a positive indication for cellulose nitrate in both cases.

Further evidence can be found by examining the IR spectra (Figure 4.10) of the unknown material compared to samples known to be cellulose nitrate. The guitar scratchplate (Rock 2725) and the accordion grill have similar spectra and are in good accordance with the prominent infrared absorption bands of cellulose nitrate [5].

5.2 steel in contact with cellulose nitrate

The physical condition of the cellulose nitrate plates was shown to have a large influence on the corrosion of steel. While the accordion grill was in good condition, the guitar scratchplate was actively degrading, showing signs of cracking. The influence on uncoated steel samples from the scratchplate and the accordion grill can be seen in figures 4.21 and 4.23 respectively. It is clear that the actively degrading cellulose nitrate releases some corrosive gases that are more intense in the places where the plate cracks, as shown in figure 4.24. This breakdown is known to increase rapidly due to radical propagation[5]. Nitrogen oxides, carbon monoxide, and carbon dioxide are compounds known to be released in the degradation process of cellulose nitrate [31, 35, 36] and an attempt was made to confirm the presence of these compounds by Raman spectroscopy, but without success. More sensitive techniques, such as mass spectrometry were inaccessible during the project. However, the observations are similar to the case of the corrosion of the surbahar in the Ringve collection.

5.3 Thin film coatings

5.3.1 Octadecyltrimethoxysilane (ODTMS)

Synthesis of ODTMS in an ethanol solution proved to be unsuccessful. Turbidity and formation of a precipitate were observed when the silane was mixed into ethanol, and the solution became unsuitable for further use. The method of synthesis chosen from the literature ([54]) used methanol which may have yielded a different result. An alternative could be to use absolute water-free ethanol.

Synthesis of ODTMS in toluene and in isopropanol resulted in clear, transparent solutions, which were used for the deposition onto the steel. The investigation of surface finishing with different cleaning methods (figure 4.9) demonstrates that the surface modification from the cleaning procedure is minimal. Comparatively, the FTIR-spectrum after the completed coating from an isopropanol solution in figure 4.7 indicates that a thin film was successfully applied to the steel surface. Most notably, the peaks at 2935 and 2859 rel.cm^{-1}. The 2922 peak is consistent with an antisymmetric C-H stretching mode of a several CH_2 group long chain, and the 2850 peak is consistent with a symmetric C-H stretching mode of a several CH2 group long chain[67, 68]

which stems from the aliphatic chain of the octadecyltrimethoxysilne molecule. Further evidence for a surface modification comes from the elemental quantification from the XPS survey scans on ODTMS-2-propanol (table 4.6), which indicates that the top 1-3 nanometers comprise ∼88% carbon, ∼6% oxygen, and ∼5% silicon. Furthermore, the fact that no Fe could be detected indicates that a film has which is thicker than a monolayer has formed. The curve fitting of the carbon 1s peak from the high resolution scan strengthens the evidence further for the silane surface layer.

The comparison of the IR spectra before coating, after coating, and after exposure to textile fabric (figure 4.2), indicating that the surface film was more or less unaffected by the exposure. This points toward a successful experiment in that the silane coating has not been removed during exposure.

The FTIR-spectrum after the completed coating from a toluene solution in figure 4.7 did indicate the same main feature for a CH_2-long chain with peaks at 2922 and 2850 rel.cm^{-1}, which stems from the aliphatic chain of The ODTMS molecule. This points toward a deposited film on the steel.

The elemental quantification from the XPS survey scans on ODTMS-toluene in table 4.6 indicates that the top 1-3 nanometers comprises ∼68% carbon, ∼26% oxygen, ∼3% silicon, ∼1% Mn, ∼1% N, and ∼1% Fe. The silicon content on the surface is lower than for ODTMS-isopropanol. The higher amount of oxygen and presence of trace elements such as Mn and N, as well as Fe, indicate that the ODTMS-toluene film is thinner than ODTMS-isopropanol.

From the visual examination, it was observed that exposure to the actively degrading cellulose nitrate scratchplate for four weeks caused both samples coated with ODTMS to corrode (figure 4.22). However, the sample coated with an isopropanol solution (sample no.2) had the best protection. The spot-wise corrosion indicates that the silane coating has a non-uniform adhesion to the substrate. ODTMS-toluene (no.4) corroded uniformly.

5.3.2 Octadecylphosphonic acid (ODPA)

The synthesis of ODPA in a toluene solution proved unsuccessful because the ODPA would not dissolve completely in the solvent. In contrast, the synthesis of ODPA in ethanol and in isopropanol resulted in clear, transparent solutions which could be used for the deposition onto the steel. The FTIR-spectrum after the completed coating from both isopropanol and ethanol solutions in figure 4.6 indicates that a thin film was successfully applied to the steel surface in both cases. The peaks at 2922 and 2850 rel.cm^{-1} related to the CH_2-long-chain molecules can again be seen, stemming. from the aliphatic chain of the ODPA molecule.

The elemental quantification from the XPS survey scans on ODPA-2-propanol in table 4.6 indicates that the top 1-3 nanometers comprise ∼81% carbon, ∼13% oxygen, ∼5% Phosphorous, ∼2% Mn and very little Fe. The high amount of carbon and phosphorous point toward the presence of ODPA on the steel surface. In comparison ODPA-ethanol had ∼71% carbon, ∼24% oxygen, ∼3% Phosphorous, ∼2% Mn and ∼0.5% Fe. The lower amount of carbon and phosphorous and the higher amount of iron indicate that the coverage of the substrate was lower in the case of ethanol as a solvent.

From the visual examination, it was observed that exposure to the actively degrading cellulose nitrate scratchplate for four weeks caused both samples coated with OPDA to corrode (figure

4.22). Both samples corroded uniformly, but it was observed that the ODPA-ethanol performed slightly better at withstaining corrosion.

5.3.3 Stearic acid (SA)

The synthesis of SA in ethanol, toluene, and isopropanol all resulted in clear, transparent solutions which could be used for the deposition onto the steel. The FTIR-spectrum after the completed coating from both the three solutions in figure 4.8 indicates that a thin film was successfully applied to the steel surface in both cases. The peaks at 2922 and 2850 rel.cm^{-1} related to the CH_2-long-chain molecules can once again be seen.

The elemental quantification from the XPS survey scans (table 4.6) showed the same basic trend for all three samples. The surfaces were found to contain ∼70% carbon, ∼24.% oxygen, ∼1.5% Mn, and 0.5% Fe. As can be seen, this is a somewhat different composition from the reference sample, meaning that there has been a change in the surface condition in all three cases.

From the visual examination, it was observed that exposure to the actively degrading cellulose nitrate scratchplate for four weeks caused all three samples coated with SA to corrode (figure 4.22). All samples corroded uniformly with SA-2-ethanol performing the best slightly better.

5.4 Investigation of square piano

No corrosion was found on the steel exposed to textile fabric during four weeks of exposure. In the previous project work [4], a possible explanation for the corrosion phenomena of steel strings in contact with textile inside the square piano was presented. The hypothesis was that presence of short-chain carboxylic acids from the breakdown of cellulose fibers.

Another possibility is that the corrosion occurs due to the release of volatile organic compounds from the casing of the square piano, as has been reported in museum artifacts elsewhere[18][19]. One argument that speaks against this is that the corrosion is not uniform inside the casing but occurs where the strings are in contact with the textile, leading to the assumption that the corrosion is caused by the textile fabric itself. Then one could argue that textiles are places where such volatile organic compounds accumulate in the instrument over the years and that the theory, therefore, still could have explanatory value for the corrosion phenomenon.

6 Conclusion

The atmospheric corrosion of steel in contact with textile fabric inside a square piano from the start of the 19th century has been investigated using a model experiment in which a corrosion protection system based on thin film organic coatings has been tested. Three types of organic thin films have been explored, ODTMS, ODPA, and SA. For each of the surface modifications, preparation from three solvents has been evaluated, toluene, isopropanol and ethanol. Surface modification of the steel has been shown by XPS and FTIR spectroscopy. Main conclusions that can be drawn from the study are summarized below.

- The preparation of ODTMS from ethanol and ODPA from toluene was unsuccessfull, whereas a modification of the steel substrate was obtained with varying for ODTMS-from isopropanol and toluene, for ODPA from ispropanol and ethanol, and SA from ispropanol, ethanol and toluene. The absence of substrate peaks in xps analysis shown that the surface modification from ODTMS resulted in a thin film thicker than a monlayer.
- In contact with nitrocellulose plates, none of the thin film coatings was sufficient to prevent rust formation, as judged by visual inspection. Overall, an optimisation of the density of the thin film coatings is required.
- Inside the square piano, no corrosion was found on the steel samples during four weeks of exposure to textile fabric. Two hypotheses for the cause the observed on iron strings are short-chain organic compounds from the degradation of textile fibers, or the release of volatile organinc compounds from he degradation of the wood casing.
- FTIR spectroscopy and a diphenylamine spot test indicated the presence of cellulose nitrate in the mandolin-banjo and surbahar, confirming the hypothesis of cellulose nitrate induced corrosion.

7 Further work

- Evaluate different preparation method of SAMs leading to denser, more protective layer, e.g. by combination with polymers.
- More detailed characterization of thin films after corrosion, e.g. by angular dependent XPS, Auger electron spectroscopy, and secondary ion mass spectrometry.
- Modify SAM preparation so that it becomes suitable for steel strings, and evaluate application in a model experiment.
- Measurement of environment inside the instrument housings for determination of air constituents such as formic acid and acetic acid, and analysis of the gases released during degradation, such as from the scratch plate by mass spectrometry.
- Conduct an experiment where the performance of thin film coatings is compared to a coating traditionally used in conservation, such as "Paraloid B72".

Bibliography

(1) Leygraf, C., *Atmospheric corrosion*; Electrochemical Society series; Wiley-Interscience: New York, 2000, pp 9–25, 192–197.

(2) Appelbaum, B., *Conservation Treatment MethodologyConservation treatment methodology*; Butterworth-Heinemann: Oxford.

(3) Ringve Musikkmuseum Taffelpiano, https://digitaltmuseum.no/011022845954/taffelpiano, Accessed: 2021-12-18.

(4) Gustad, F. E. *Specialization Project, NTNU* **2021**.

(5) Bussiere, P.-O.; Gardette, J.-L.; Therias, S. *Polymer Degradation and Stability* **2014**, *107*, 246–254.

(6) Springate, M. E. *Northeast Historical Archaeology* **1997**, *26*, 5.

(7) De Bruyn-Ouboter Vera, C. a. R. m. m., personal communication.

(8) Rasmussen, S. C. *ANGEWANDTE CHEMIE-INTERNATIONAL EDITION* **2021**, *60*, 8012–8016.

(9) Surbahār, eng, 2011.

(10) Newbury, B. D.; Notis, M. R. *JOM (1989)* **2004**, *56*, 33–37.

(11) Goodway, M.; Odell, S., *The metallurgy of 17th- and 18th- century music wire*; 3. Vol. Volume 2, Pendragon press: Stuyvesant, NY, 1987, pp 15–30.

(12) Petrucci, R. H., *General chemistry : principles and modern applications*, 11th ed.; Pearson Canada Inc.: Toronto, 2016, pp 167–169.

(13) Oldham, K.; Myland, J.; Bond, A., *Electrochemical Science and Technology: Fundamentals and Applications*; John Wiley & Sons, Incorporated: Hoboken, 2011, pp 213–230.

(14) Cicek, V., *Corrosion chemistry*; Wiley Scrivener: Hoboken, N.J., 2011, pp 15–21.

(15) Landolt, D., *Corrosion and surface chemistry of metals*; EPFL Press: Lausanne, 2007, pp 12–44, 343–359.

(16) Callister, W. D., *Materials science and engineering*, 9th ed., SI Version.; Wiley: Hoboken, N.J, 2015, p 655.

(17) *Encyclopedia of electrochemistry : Vol. 4 : Corrosion and oxide films*; Wiley-VCH: Weinheim, 2003; Vol. Vol. 4, p 192.

(18) Prosek, T.; Taube, M.; Dubois, F.; Thierry, D. *Corrosion Science* **2014**, *87*, 376–382.

(19) Ryhl-Svendsen, M.; Glastrup, J. *Atmospheric Environment* **2002**, *36*, 3909–3916.

(20) Chawla, K. K., *Fibrous materials*; Cambridge solid state science series; Cambridge University Press: Cambridge, 1998, pp 19, 43–45, 50–53.

(21) Duprat, C. *Annual Review of Fluid Mechanics* **2022**, *54*, 444–467.

(22) Saunders, K. J., *Organic polymer chemistry : an introduction to the organic chemistry of adhesives, fibres, paints, plastics and rubbers*, 2nd ed.; Chapman and Hall: London, 1988, p 216.

(23) Solomons, T. W. G., *Organic chemistry*, 11th ed.; Wiley: Singapore, 2014, p 1061.

(24) Morad, M. S. *JOURNAL OF APPLIED ELECTROCHEMISTRY* **2008**, *38*, 1509–1518.

(25) Oezcan, M. *JOURNAL OF SOLID STATE ELECTROCHEMISTRY* **2008**, *12*, 1653–1661.

(26) John M., M., *Organic Chemistry : Fundamentals and Concepts.* De Gruyter Textbook; De Gruyter: 2018, p 130.

(27) Umoren, S. A.; AlAhmary, A. A.; Gasem, Z. M.; Solomon, M. M. *INTERNATIONAL JOURNAL OF BIOLOGICAL MACROMOLECULES* **2018**, *117*, 1017–1028.

(28) Michal, J.; Katarina, H.; Svetozar, K.; Jozef, L.; Martina, B. *Cellulose chemistry and technology* **2012**, *46*, 331–340.

(29) Horrocks, A. R., *Handbook of technical textiles : Volume 1, : Technical textile processes*, 2nd ed.; Woodhead publishing in textiles, Vol. Volume 1, Woodhead Publishing in association with The Textile Institute: Amsterdam, Netherlands, 2016, pp 231–234, 239–251.

(30) Zollinger, H., *Color chemistry : syntheses, properties and applications of organic dyes and pigments*, 3rd, rev. ed.; Verlag Helvetica Chimica Acta: Zürich, 2003, pp 15–30.

(31) Waentig, F., *Plastics in art : a study from the conservation point of view*; Michael Imhof Verlag: Petersberg, 2008, pp 202–216.

(32) Li, L.; Frey, M. *Polymer* **2010**, *51*, 3774–3783.

(33) Carter, E. A.; Swarbrick, B.; Harrison, T. M.; Ronai, L. *Heritage Science* **2020**, *8*, 1–13.

(34) Canaidain Conservation Instituion. The Diphenylamine spot test for cellulose nitrate in museum objects, Canadian Conservation Instituion Notes, 17/2, 1994.

(35) Berthumeyrie, S.; Collin, S.; Bussiere, P.-O.; Therias, S. *Journal of Hazardous Materials* **2014**, *272*, 137–147.

(36) Nunes, S.; Ramacciotti, F.; Neves, A.; Angelin, E. M.; Ramos, A. M.; Roldao, E.; Wallaszkovits, N.; Armijo, A. A.; Melo, M. J. *HERITAGE SCIENCE* **2020**, *8*, DOI: 10.1186/s40494-020-00373-4.

(37) Abrantes, L.; Melato, A. In *Corrosion and Conservation of Cultural Heritage Metallic Artefacts*, Dillmann, P., Watkinson, D., Angelini, E., Adriaens, A., Eds.; European Federation of Corrosion (EFC) Series; Woodhead Publishing: 2013, pp 518–539.

(38) Ntelia, E.; Karapanagiotis, I. *Progress in Organic Coatings* **2020**, *139*, 105224.

(39) Kovács, R. L.; Daróczi, L.; Barkóczy, P.; Baradács, E.; Bakonyi, E.; Kovács, S.; Erdélyi, Z. *Journal of Coatings Technology and Research* **2020**, *18*, 523–534.

(40) Frey, H.; Khan, H. R., *Handbook of Thin Film Technology*, 1st ed.; Springer Berlin / Heidelberg: Berlin, Heidelberg, 2015.

(41) Pehkonen, S. O.; Yuan, S. In *Tailored Thin Coatings for Corrosion Inhibition using a Molecular Approach*, Pehkonen, S. O., Yuan, S., Eds.; Interface Science and Technology, Vol. 23; Elsevier: 2018, pp 13–21.

(42) Ashkenazi, D.; Nusbaum, I.; Shacham-Diamand, Y.; Cvikel, D.; Kahanov, Y.; Inberg, A. *Corrosion Science* **2017**, *123*, 88–102.

(43) Ulman, A. *Chemical Reviews* **1996**, *96*, PMID: 11848802, 1533–1554.

(44) Schreiber, F. *Progress in Surface Science* **2000**, *65*, 151–257.

(45) Raman, A.; Quiñones, R.; Barriger, L.; Eastman, R.; Parsi, A.; Gawalt, E. S. *Langmuir* **2010**, *26*, PMID: 20039608, 1747–1754.

(46) Kuznetsov, Y. I. *INTERNATIONAL JOURNAL OF CORROSION AND SCALE INHIBITION* **2017**, *6*, 384–427.

(47) Liakos, I. L.; Newman, R. C.; McAlpine, E.; Alexander, M. R. *Langmuir* **2007**, *23*, PMID: 17241003, 995–999.

(48) Foster, T. T.; Alexander, M. R.; Leggett, G. J.; McAlpine, E. *Langmuir* **2006**, *22*, PMID: 17042539, 9254–9259.

(49) Spori, D. M.; Venkataraman, N. V.; Tosatti, S. G. P.; Durmaz, F.; Spencer, N. D.; Zürcher, S. *Langmuir* **2007**, *23*, PMID: 17569549, 8053–8060.

(50) Petrunin, M. A.; Gladkikh, N. A.; Maleeva, M. A.; Maksaeva, L. B.; Yurasova, T. A. *INTERNATIONAL JOURNAL OF CORROSION AND SCALE INHIBITION* **2019**, *8*, 882–907.

(51) van Ooij, W.; Zhu, D.; Stacy, M.; Seth, A.; Mugada, T.; Gandhi, J.; Puomi, P. *Tsinghua Science & Technology* **2005**, *10*, 639–664.

(52) Ohkubo, H.; Itoh, J.; Nagano, H.; Koura, T.; Kawase, M.; Takahagi, T. *Zairyo-to-Kankyo* **2003**, *52*, 316–318.

(53) Liakos, I. L.; Newman, R. C.; McAlpine, E.; Alexander, M. R. *Surface and Interface Analysis* **2004**, *36*, Cited by: 82, 347–354.

(54) Al-Saadi, S.; Singh Raman, R. *Progress in Organic Coatings* **2019**, *127*, 27–36.

(55) PETRUNIN, M.; NAZAROV, A.; MIKHAILOVSKII, Y. *Protection of metals : official English translation of Zashchita metallov* **1990**, *26*, 587–592.

(56) Keller, H.; Rengel, H.; Poganiuch, P. *Journal of Magnetism and Magnetic Materials* **1996**, *155*, International Conference on Magnetic Recording Media, 101–103.

(57) Mingalyov, P. G.; Lisichkin, G. V. *Russian chemical reviews* **2006**, *75*, 541–557.

(58) Kosian, M.; Smulders, M. M. J.; Zuilhof, H. *Langmuir* **2016**, *32*, PMID: 26771302, 1047–1057.

(59) Jadhav, S. *Open Chemistry* **2011**, *9*, 369–378.

(60) Marusic, K.; Hajdari, Z.; Curkovic, H. O. *ACTA CHIMICA SLOVENICA* **2014**, *61*, 328–339.

(61) Shustak, G.; Domb, A. J.; Mandler, D. *Langmuir* **2004**, *20*, PMID: 15323494, 7499–7506.

(62) Raman, A.; Gawalt, E. S. *Langmuir* **2007**, *23*, PMID: 17266343, 2284–2288.

(63) Long, D. A. *Journal of Raman spectroscopy* **2005**, *36*, 271–271.

(64) Erbe, A.; Nayak, S.; Chen, Y.-H.; Niu, F.; Pander, M.; Tecklenburg, S.; Toparli, C. In *Encyclopedia of Interfacial Chemistry*, Wandelt, K., Ed.; Elsevier: Oxford, 2018, pp 199–219.

(65) Kaufmann, C. R.; Mani, G.; Marton, D.; Johnson, D. M.; Agrawal, C. M. *BIOMEDICAL MATERIALS* **2010**, *5*, DOI: 10.1088/1748-6041/5/2/025008.

(66) Raman, A.; Dubey, M.; Gouzman, I.; Gawalt, E. S. *LANGMUIR* **2006**, *22*, 6469–6472.

(67) SNYDER, R.; STRAUSS, H.; ELLIGER, C. *JOURNAL OF PHYSICAL CHEMISTRY* **1982**, *86*, 5145–5150.

(68) MACPHAIL, R.; STRAUSS, H.; SNYDER, R.; ELLIGER, C. *JOURNAL OF PHYSICAL CHEMISTRY* **1984**, *88*, 334–341.

Appendix

A XPS measurements

A.1 Survey scans

Table A.1: XPS aquisition parameters for survey scan and high resolution scans.

Measurement	Sweeps	Dwell time [ms]	Interval
Survey	3	100	1
Fe	5	200	0.1
O	3	350	0.1
N	7	300	0.1
Ca	7	450	0.1
S	7	300	0.1
C	3	100	0.1
P	3	300	0.1
Si	3	200	0.1

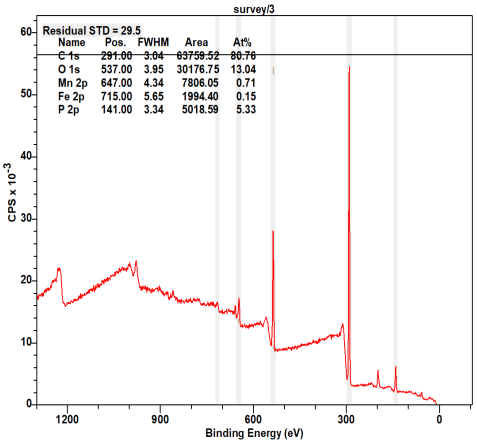

Figure A.1: Quantification from survey scan of sample ODPA-2-propanol

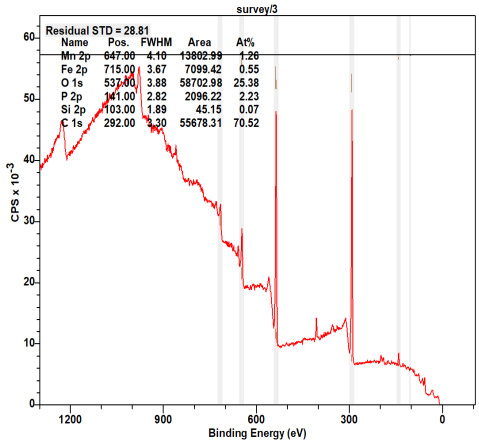

Figure A.2: Quantification from survey scan of sample ODPA-D

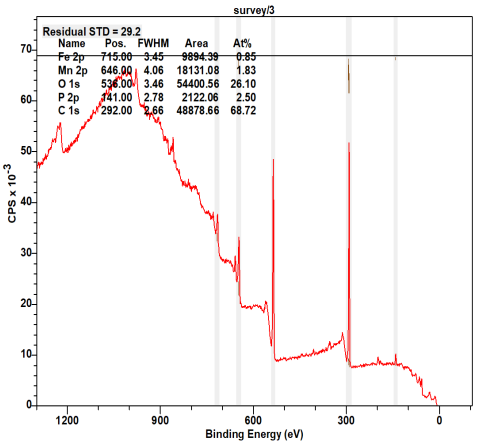

Figure A.3: Quantification from survey scan of sample ODPA-L

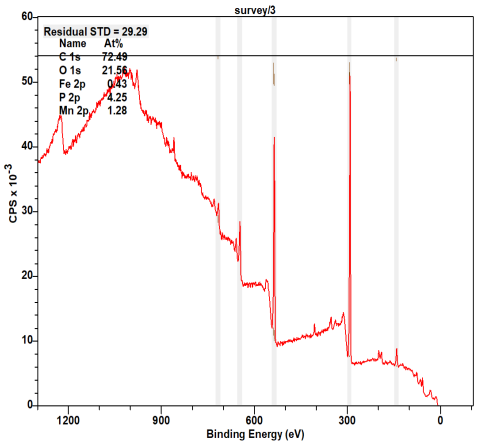

Figure A.4: Quantification from survey scan of sample ODPA-RL

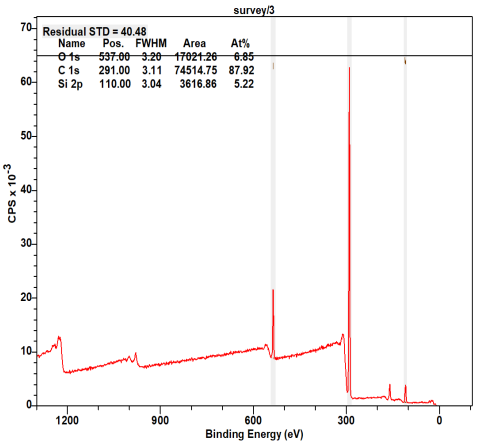

Figure A.5: Quantification from survey scan of sample ODTMS-2-propanol

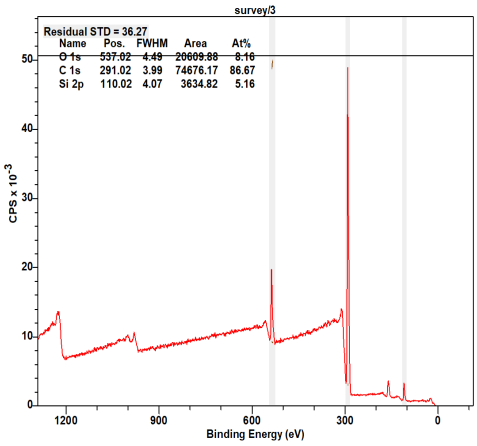

Figure A.6: Quantification from survey scan of sample ODTMS-D

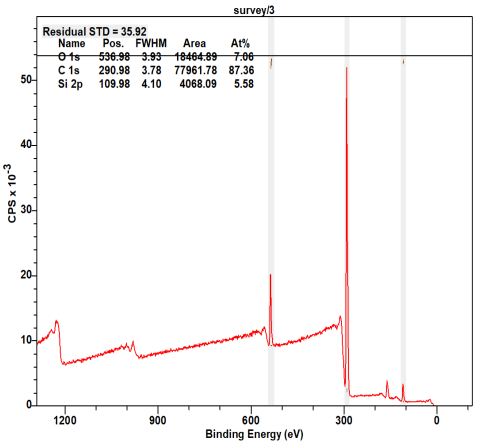

Figure A.7: Quantification from survey scan of sample

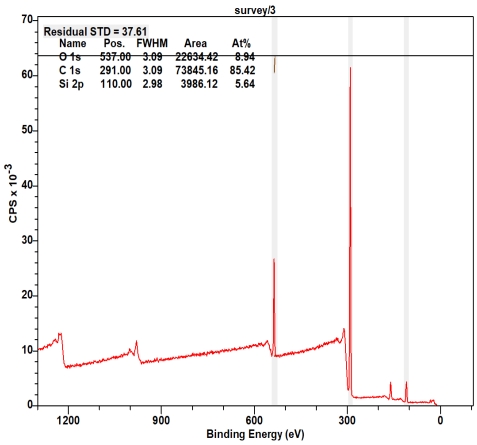

Figure A.8: Quantification from survey scan of sample ODTMS-RL

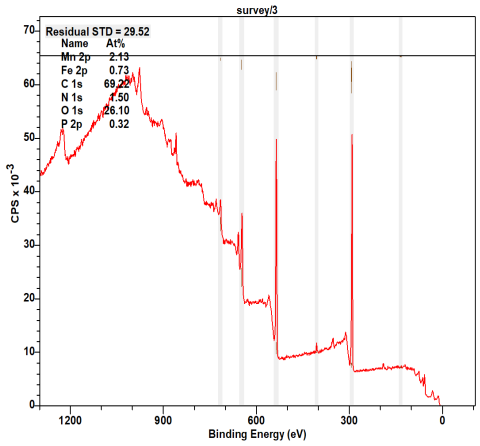

Figure A.9: Quantification from survey scan of sample SA-2-propanol

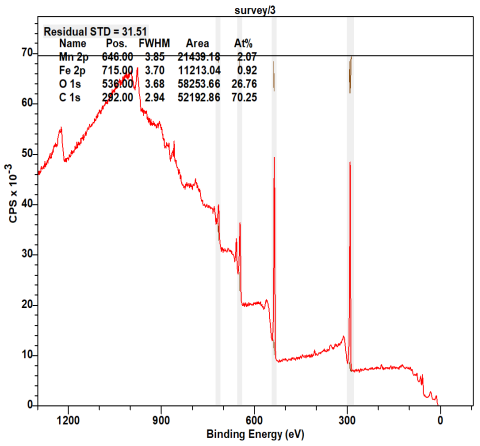

Figure A.10: Quantification from survey scan of sample SA-D

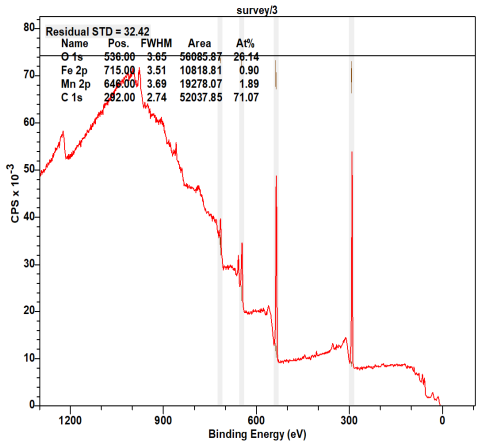

Figure A.11: Quantification from survey scan of sample SA-L

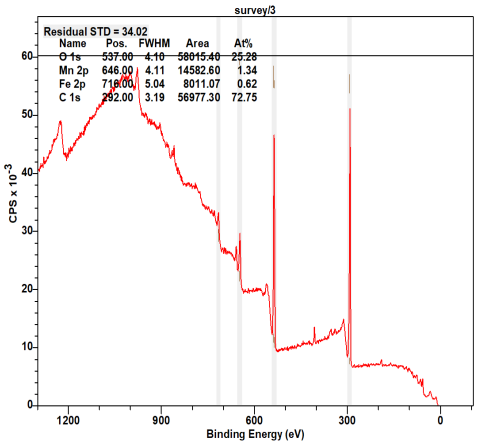

Figure A.12: Quantification from survey scan of sample SA-RL

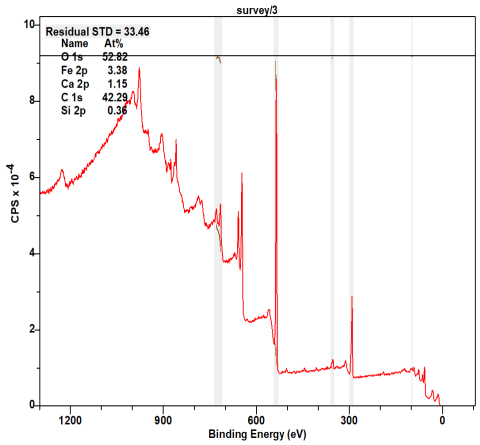

Figure A.13: Quantification from survey scan of sample U-D

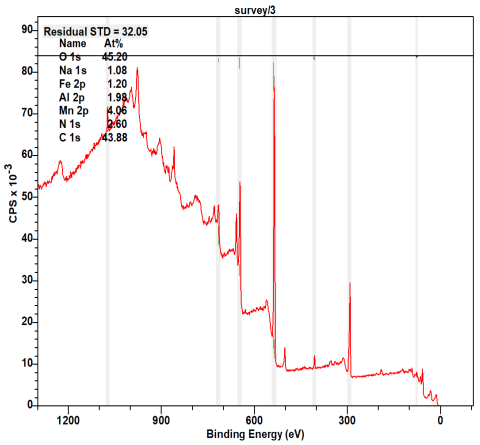

Figure A.14: Quantification from survey scan of sample U-RL

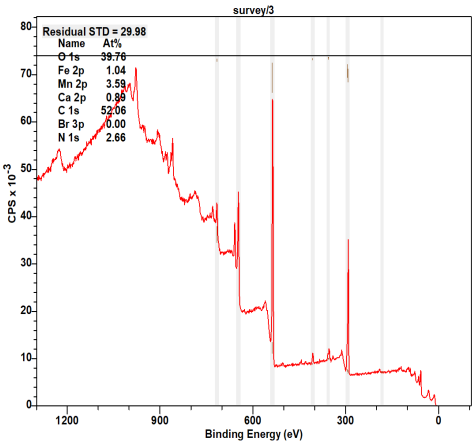

Figure A.15: Quantification from survey scan of sample U-L

A.2 Carbon 1s High resolution scans

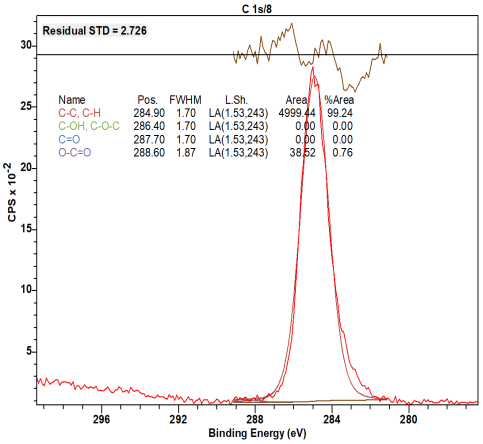

Figure A.16: Peak fit for carbon 1s peak for sample ODPA-2-propanol

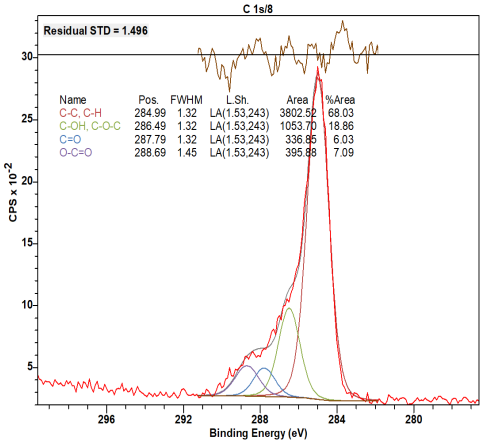

Figure A.17: Peak fit for carbon 1s peak for sample ODPA-D

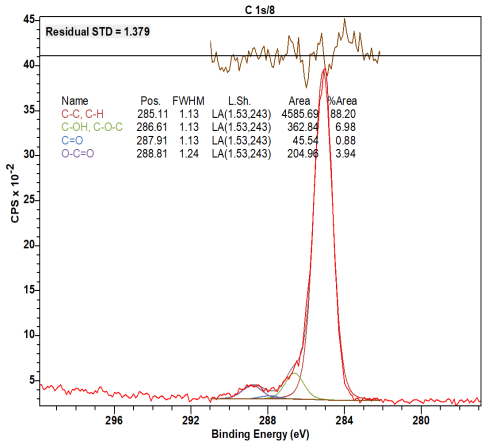

Figure A.18: Peak fit for carbon 1s peak for sample ODPA-L

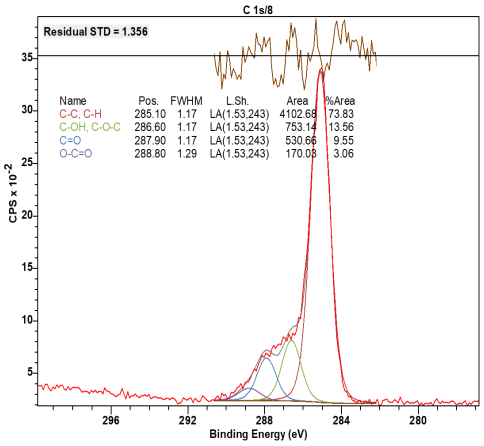

Figure A.19: Peak fit for carbon 1s peak for sample ODPA-RL

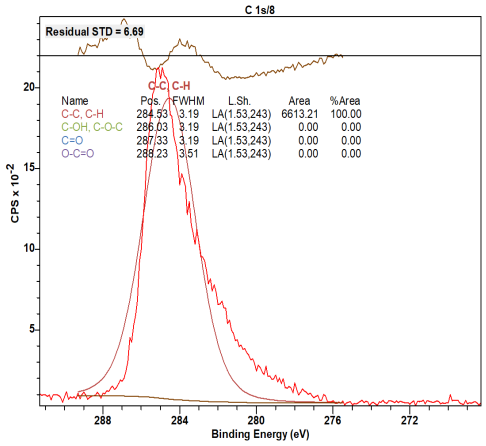

Figure A.20: Peak fit for carbon 1s peak for sample ODTMS-D

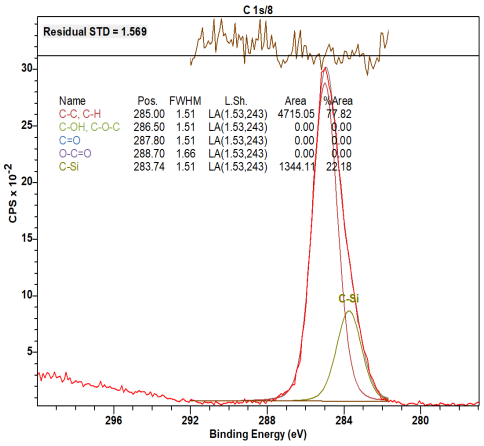

Figure A.21: Peak fit for carbon 1s peak for sample ODTMS-2-propanol

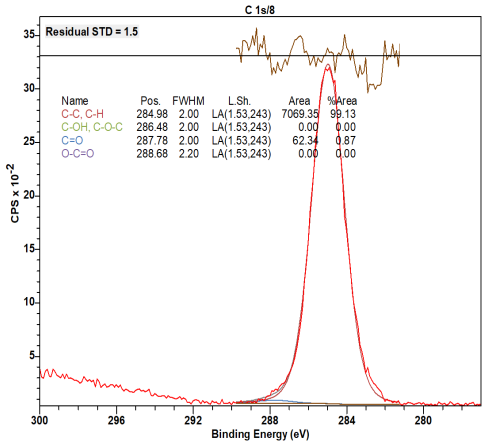

Figure A.22: Peak fit for carbon 1s peak for sample ODTMS-RL

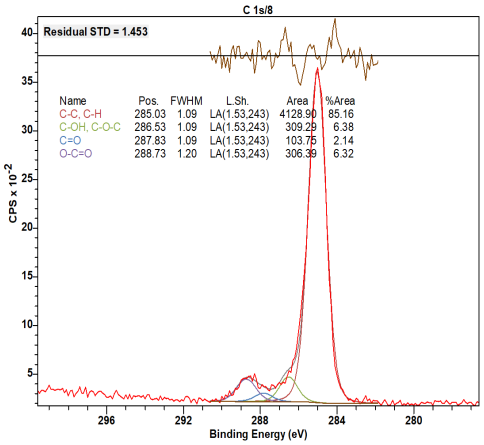

Figure A.23: Peak fit for carbon 1s peak for sample SA-2-propanol

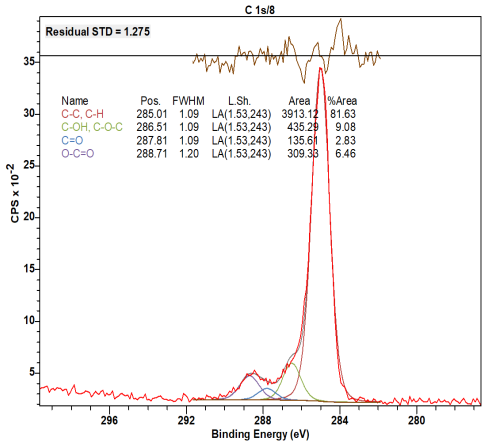

Figure A.24: Peak fit for carbon 1s peak for sample SA-D

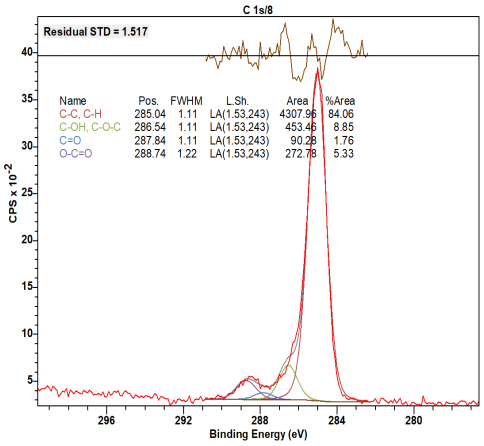

Figure A.25: Peak fit for carbon 1s peak for sample

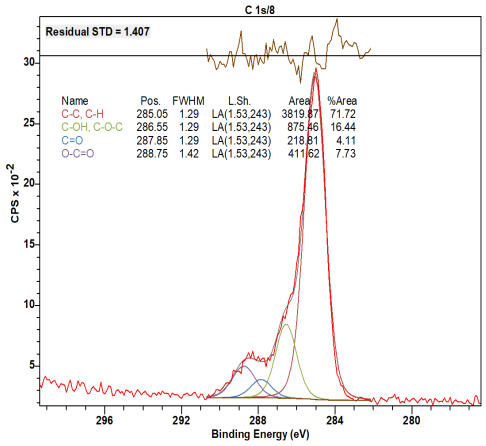

Figure A.26: Peak fit for carbon 1s peak for sample SA-RL

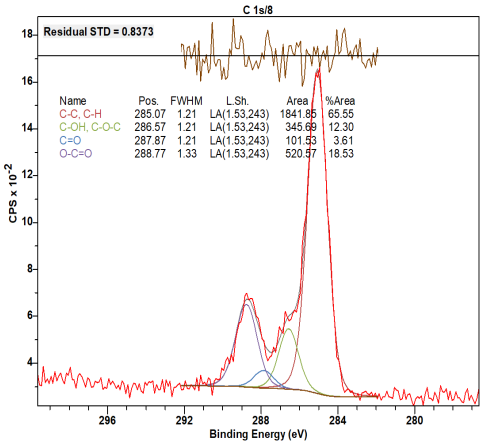

Figure A.27: Peak fit for carbon 1s peak for sample U-D

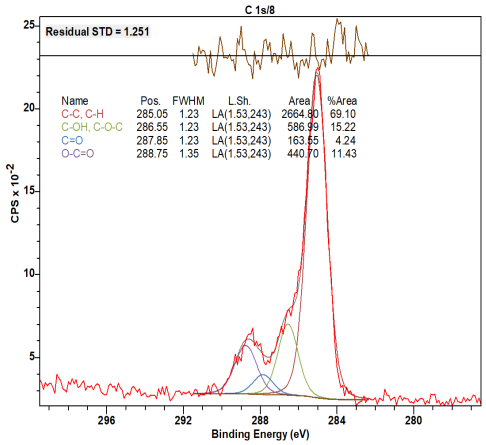

Figure A.28: Peak fit for carbon 1s peak for sample U-L

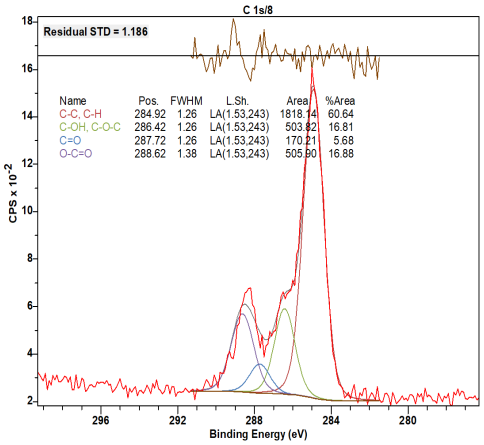

Figure A.29: Peak fit for carbon 1s peak for sample U-RL

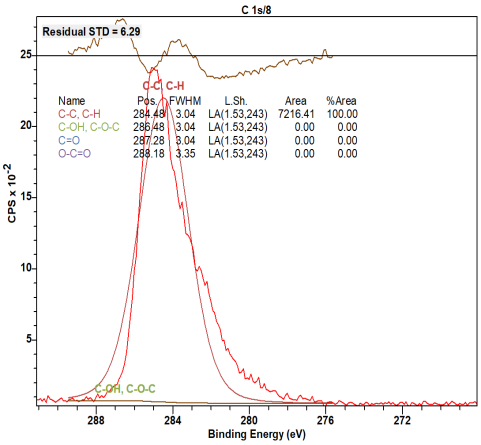

Figure A.30: Peak fit for carbon 1s peak for sample ODTMS-L

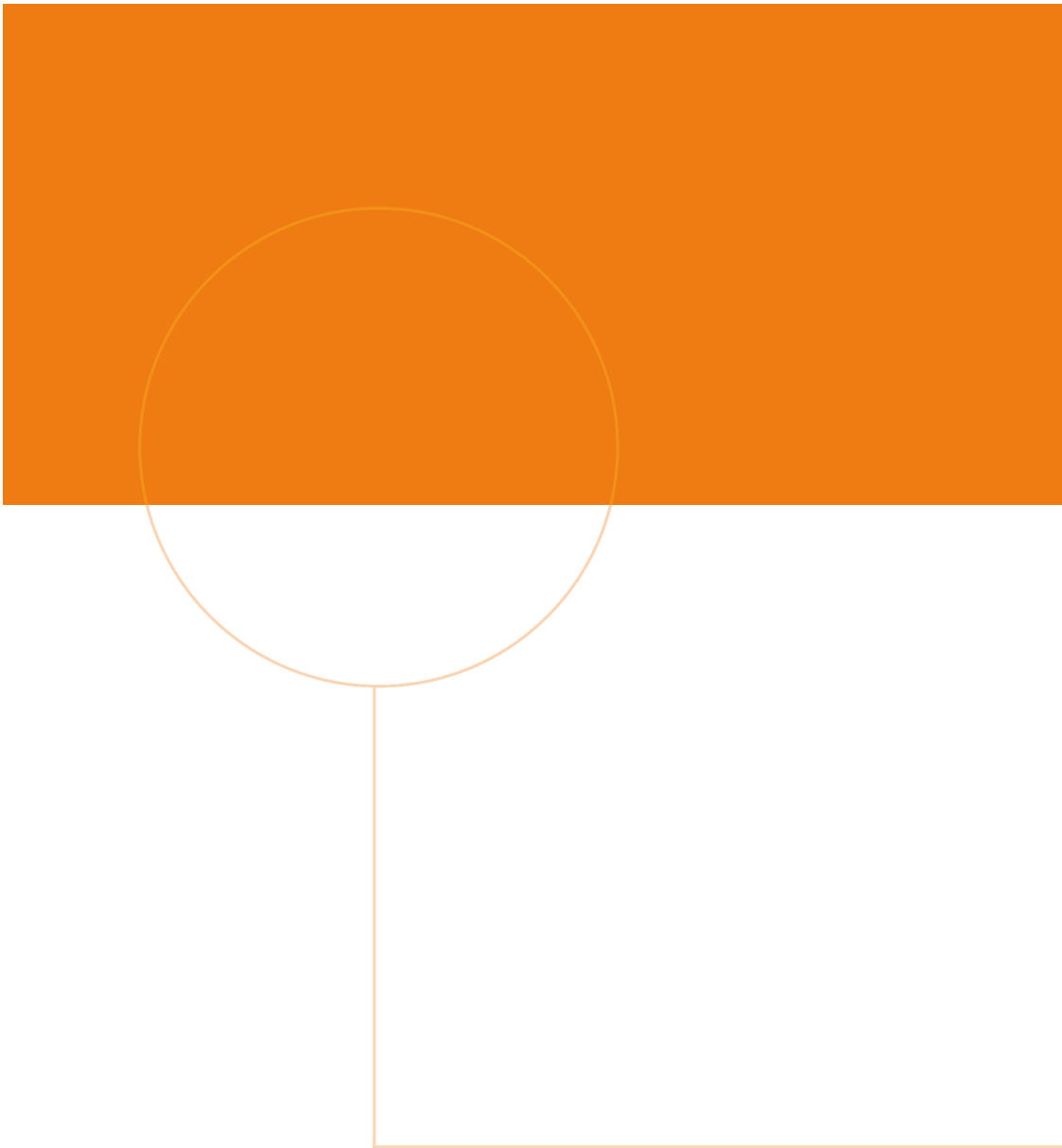

NTNU

Norwegian University of
Science and Technology